bioRxiv preprint doi: https://doi.org/10.1101/249227; this version posted January 16, 2018. The copyright holder for this preprint (which was not certified by peer review) is the author/funder. All rights reserved. No reuse allowed without permission.

TMEM16F activation by Ca^{2+} triggers plasmalemma expansion and directs PD-1 trafficking

Christopher Bricogne[1]*, Michael Fine[2]*, Pedro M. Pereira[3], Julia Sung[4], Maha Tijani[4], Ricardo Henriques[3], Mary K Collins[1,4,5]*† and Donald Hilgemann[2]†

Author Affiliation:

[1] UCL Cancer Institute, University College London, Gower St, London, UK.

[2] University of Texas Southwestern Medical Center, Department of Physiology, Dallas, Texas, USA

[3] MRC Laboratory for Molecular Cell Biology, University College London, Gower St, London, UK

[4] National Institute for Biological Standards and Control, Blanche Lane, South Mimms, Herts, UK

[5] Present Address since September 2016, Okinawa Institute of Science and Technology, Onna-son, Okinawa, Japan

Corresponding Author: Donald.hilgemann@utsouthwestern.edu

Orchid ID 0000-0002-5288-5133

Co-corresponding Author: mary.collins@oist.jp;

Orcid ID 0000-0002-9539-0130.

* These authors contributed equally to the work

† These authors contributed equally to the work

bioRxiv preprint doi: https://doi.org/10.1101/249227; this version posted January 16, 2018. The copyright holder for this preprint (which was not certified by peer review) is the author/funder. All rights reserved. No reuse allowed without permission.

Abstract

TMEM16F, an ion channel gated by high cytoplasmic Ca^{2+}, is required for cell surface phosphatidylserine exposure during platelet aggregation and T cell activation. Here we demonstrate in Jurkat T cells and HEK293 cells that TMEM16F activation triggers large-scale surface membrane expansion in parallel with lipid scrambling. Following TMEM16F mediated scrambling and surface expansion, cells undergo extensive membrane shedding. The membrane compartment that expands the cell surface does not recycle, nor does it involve endoplasmic reticulum or acidified lysosomes. Surprisingly, T cells lacking TMEM16F expression not only fail to scramble lipid and expand surface membrane, but instead undergo a rapid membrane internalization known as massive endocytosis (MEND) in response to the same Ca^{2+} stimulus as their parental cells. TMEM16F dependent membrane shedding and MEND traffic similar sets of membrane receptors from the cell surface. The selective participation of the T cell co-receptor PD-1 in this trafficking is determined by its single transmembrane domain, establishing a fundamental role for TMEM16F as a regulator of Ca^{2+}-activated membrane trafficking.

bioRxiv preprint doi: https://doi.org/10.1101/249227; this version posted January 16, 2018. The copyright holder for this preprint (which was not certified by peer review) is the author/funder. All rights reserved. No reuse allowed without permission.

Introduction

Eukaryotic cells sequester phosphatidylserine (PS) into the cytoplasmic leaflet of the plasma membrane (Leventis and Grinstein, 2010). PS becomes exposed in the outer plasmalemma leaflet in response to cytoplasmic Ca^{2+} elevations and during the execution of apoptosis (Bevers and Williamson, 2010).

Recent work indicates that the response to Ca^{2+} elevation is mediated by the Ca^{2+}-activated ion channel, TMEM16F (or Anoctamin 6), a widely expressed member of the TMEM16 family (Schreiber et al., 2010). In platelets, this type of PS exposure is an important step in blood coagulation (Suzuki et al., 2010; Yang et al., 2012), and the overt phenotype caused by TMEM16F mutations in humans is a bleeding disorder known as Scott Syndrome (Yang et al., 2012). TMEM16F activation in T-cells is proposed to restrict receptor responses during chronic infection (Hu et al., 2016). In contrast, PS exposure during apoptosis, which marks cells for removal by phagocytosis (Marino and Kroemer, 2013), is not dependent on TMEM16F and may not require Ca^{2+} signals (Suzuki et al., 2010).

Crystal structures of a fungal TMEM16F orthologue reveal a hydrophilic groove (Brunner et al., 2014) that might serve as a conduit for both ions and lipids to pass through the TMEM16F channel, and reconstitution experiments using the fungal TMEM16F support this interpretation (Malvezzi et al., 2013; Brunner et al., 2014). In agreement with this model, a 35 amino acid “scrambling” domain identified in TMEM16F is part of this hydrophilic cleft (Gyobu et al., 2015; Yu et al., 2015). These findings are closely consistent with TMEM16F acting as both an ion channel and lipid “scramblase”, whereby both ions and lipids permeate the channel pore.

In addition to its role in PS exposure, effects of TMEM16F activity on membrane trafficking have been reported. TMEM16F is involved in microvesicular ectosome release from platelets and neutrophils (Headland et al., 2015), and in macrophages TMEM16F is necessary for phagocytosis stimulated by the ATP receptor $P2X_7$ (Ousingsawat et al., 2015a). Mice lacking TMEM16F also show deficits in bone development (Ousingsawat et al., 2015b), a process that has been linked to microvesicles (Anderson, 2003). Microglia lacking TMEM16F demonstrate defects in process formation and phagocytosis (Batti et al., 2016). Finally, mice lacking TMEM16F suffer from immune exhaustion, at least in part due to a failure to down-regulate PD-1, leading to a failure to clear viral infections

bioRxiv preprint doi: https://doi.org/10.1101/249227; this version posted January 16, 2018. The copyright holder for this preprint (which was not certified by peer review) is the author/funder. All rights reserved. No reuse allowed without permission.

(Hu et al., 2016).

We have described previously that PS exposure can occur in close association with large exocytic responses activated by elevating cytoplasmic free Ca^{2+} to greater than 10 μM in fibroblasts(Yaradanakul et al., 2008). We therefore examined the role of TMEM16F in Ca^{2+}-induced membrane expansion. We describe here in both Jurkat T cells and HEK293 cells that cytoplasmic Ca^{2+} elevations cause rapid surface membrane expansion in close parallel with PS exposure and the opening of TMEM16F channels. The absence of TMEM16F blocks both exocytosis and PS exposure. Surprisingly, the absence of TMEM16F promotes massive endocytosis (MEND) (Lariccia et al., 2011) over the same time course that membrane expansion would have occurred.

Given the novel observation that TMEM16F controls large-scale membrane trafficking events, we next examined whether specific surface proteins traffic with the corresponding membrane movements. We show in T cells that the immune response regulator PD-1 is selectively shed in vesicles after TMEM16F activation, while it is selectively internalized in the absence of TMEM16F during MEND. This preferential trafficking is dependent on the transmembrane region of PD-1, indicating that the intramembrane segment of PD-1 promotes its participation in membrane domains that can be either shed as ectosomes or internalized via MEND. These results provide a potential explanation for the TMEM16F regulation of PD-1 cell surface expression changes described previously (Hu et al., 2016). As PD-1 is a negative regulator of the immune system, which can be hijacked by various cancers to evade intrinsic immune responses, antibodies that block its function are considered potent cancer therapeutics (Pardoll, 2012). Thus the Ca^{2+}- and TMEM16F-dependent regulation of PD-1 expression in the cell surface may be of immunological and clinical significance.

bioRxiv preprint doi: https://doi.org/10.1101/249227; this version posted January 16, 2018. The copyright holder for this preprint (which was not certified by peer review) is the author/funder. All rights reserved. No reuse allowed without permission.

Results

TMEM16F regulates large Ca^{2+}-activated surface membrane expansion.

To delete TMEM16F in Jurkat T cells we employed a CRISPR/Cas9 lentiviral vector. We confirmed by genomic DNA sequencing that all TMEM16F copies in Jurkat T cells were mutated, leading to proteins truncated in Exon 2 or 5 (**Figure 1–figure supplement 1**). Commercial TMEM16F antibodies were not reliable for Western blotting, whether employing whole lysates or membrane preparations. Therefore, we employed proteomic analysis of membrane preparations to confirm the quantitative loss of TMEM16F in Jurkat cells (**Figure 1–figure supplement 2**). To determine whether TMEM16F is required for Ca^{2+} mediated PS exposure, we treated cells with the Ca^{2+} ionophore ionomycin and performed fluorescence-activated cell sorting (FACS). Cells with increased cytoplasmic Ca^{2+} were detected via an increase of Fluo4 fluorescence, and cells with PS exposure were dectected via Annexin V staining (**Figure 1**). WT cells responded to ionomycin by correlated increases of cytoplasmic Ca^{2+} and Annexin V binding. Cytoplasmic Ca^{2+} increased in TMEM16F-null cells to the same extent as in WT cells, but TMEM16F-null cells failed to externalize PS, confirming the role of TMEM16F in Ca^{2+}-activated PS scrambling (Hu et al., 2016). The Exon 2 truncated TMEM16F-null line was employed in subsequent experiments.

For real-time analysis of the surface membrane in Jurkat cells, we employed simultaneously patch clamp recording and confocal imaging. Plasmalemma (PM) conductance (G_m) and capacitance (C_m) were monitored via continuous square wave voltage perturbation. Membrane area is proportional to C_m, while G_m quantifies the voltage-dependent permeation of ions through the membrane. The surface binding of an impermeable fluorescent membrane dye, FM4-64, was monitored optically. During a 20s exposure of Jurkat T cells to the Ca^{2+} ionophore, ionomycin (5μM), the PM area doubles on average (**Figure 2A**, C_m red trace), and FM4-64 dye binding increases by nearly three-fold (**Figure 2A**, **Figure 2-figure supplement 1**). FM4-64 binding reverses rapidly when the dye is removed, indicating that the dye does not significantly enter cells (**Figure 2A-4)**. In contrast to canonical exocytosis, which indeed occurs in T lymphocytes (Matti et al., 2013), membrane expansion in these experiments was insensitive to VAMP2 cleavage by tetanus toxin and did not require cytoplasmic ATP or (**Figure 2C**). Simultaneous with the onset of membrane expansion, the PM conductance of Jurkat T cells increased substantially and declined nearly to baseline in parallel with

bioRxiv preprint doi: https://doi.org/10.1101/249227; this version posted January 16, 2018. The copyright holder for this preprint (which was not certified by peer review) is the author/funder. All rights reserved. No reuse allowed without permission.

the asymptotic rise of C_m (**Figure 2A**. G_m, blue trace). Relationships between ion conduction via TMEM16F and membrane expansion are analysed in detail in an accompanying article.

In TMEM16F-null cells, the Ca^{2+}-activated increase of conductance was abolished (**Figure 2B**, blue trace). Likewise, instead of expanding by two-fold the PM area decreased by 50% over 25s (**Figure 2B**, red trace). That this decrease reflects extensive endocytosis is established unambiguously by the fact that FM4-64 binding does not reverse after dye is washed off. Rather, the dye becomes locked into membrane structures below the cell surface (**Figure 2B-4, Figure 2–figure supplement 2)**. These observations are all consistent with the occurrence of a rapid form of Ca^{2+} activated massive endocytosis (MEND) that we have described previously in fibroblasts (Lariccia et al., 2011). Similar to MEND, these endocytic responses are not blocked by inhibiting clathrin or dynamin, nor by perturbing the actin cytoskeleton with latrunculin or phalloidin (**Figure 2D**).

Further evidence that TMEM16F activity initiates membrane expansion involvement is provided in **Figure 3.** Our previous work demonstrated that cytoplasmic polyamines, such as spermidine and spermine, can switch Ca^{2+}-induced membrane expansion to massive endocytic (MEND) responses in fibroblasts (Lariccia et al., 2011), very similar to the effects of TMEM16F deletion. As shown in **Figure 3A**, spermine at physiological concentrations (200 to 500 μM) also switches the Jurkat WT Ca^{2+} response to MEND. Impressively, the TMEM16F conductance is blocked by spermine in close parallel with the switch to MEND, and we point out that spermine has been described to block phospholipid scrambling in red blood cells that lack internal membranes (Bratton, 1994). Accordingly, these data are consistent with the idea that phospholipid scrambling by TMEM16F is linked to the membrane expansion responses.

The origins of membrane that expands the cell surface.

We next set out to determine what intracellular compartments could contribute to such a large expansion of surface membrane. We looked for evidence of fusion of recycled intracellular vesicles in Jurkat T cells by utilizing super-resolution confocal microscopy projections of intact cells and PM surface imaging with Total Internal Reflection Fluorescence microscopy (TIRF). Jurkat cells were incubated with FM4-64 for 1 hour to

bioRxiv preprint doi: https://doi.org/10.1101/249227; this version posted January 16, 2018. The copyright holder for this preprint (which was not certified by peer review) is the author/funder. All rights reserved. No reuse allowed without permission.

label internalized endosomes, washed to remove extracellular dye, and attached to fibronectin coated dishes. **Figure 4A** describes 0.75 µm z-plane sections projected unto a 2D pictograph to reveal significant FM dye labelling of sub-micron vesicles throughout the cytoplasm. After 5 minutes of treatment with ionomycin there was no significant change in the number of particles observed indicating that the majority of internally labelled recycled membrane does not participate in our observed membrane expansion (**Figure 4B**). Interestingly, we routinely observed rapid movements of punctae directly after ionomycin application. Coupled with the lack of a significant change in the total number of punctae and the slow temporal resolution of 3D high resolution microscopy this might indicate that sorting of particles occurs rapidly and a subset of labelled membrane near the surface of the cell may still be involved. These fast-moving labelled punctae may fuse back to the surface, but are masked by the large signal that remains entirely cytoplasmic.

To examine if a subset of vesicles near the surface could account for the large amounts of novel membrane exposed during TMEM16F activation, we labelled Jurkat and Jurkat TMEM16F-null cells with FM 4-64, as before, and analysed punctae loss using TIRF microscopy, as previously described (**Figure 4C**) (Zhang et al., 2007). For WT cells, the number of FM-dye stained punctae per cell significantly decreased after Ca^{2+}-ionophore by 30% over 5 minutes. DMSO treated control cells displayed a 14% increase in the number of punctae observed. (**Figure 4D**). TMEM16F-null cells showed no significant loss of punctae in response to Ca^{2+}-ionophore treatment versus DMSO (**Figure 4D**). While results are consistent with TMEM16F in some way promoting the fusion of recycling endosomes, the extent and rate of events visualized via TIRF fall far short of accounting for the doubling of membrane area detected as an increase in C_m (**Figure 2A**). Thus, additional membrane must contribute to the large PM expansion.

Lysosomal compartments are described to fuse to the cell surface during cell wounding (Reddy et al., 2001), and the endoplasmic reticulum (ER) represents a very large repository of intracellular membrane close to the cell surface. To determine if our observed increases in cell surface involved fusion of these intracellular compartments to the surface membrane we expressed fluorescently tagged STIM1 (an ER resident protein) and used LysoTracker to label acidified lysosomes. If ER membrane became contiguous with the surface, the luminal YFP tagged to STIM1 would become exposed to the extracellular solution. Once exposed, the presence of the impermeable quencher

bioRxiv preprint doi: https://doi.org/10.1101/249227; this version posted January 16, 2018. The copyright holder for this preprint (which was not certified by peer review) is the author/funder. All rights reserved. No reuse allowed without permission.

Trypan Blue in the extracellular buffer would reduce YFP fluorescence intensity (Wan et al., 1993). Likewise, Lysotracker® is a soluble fluorescent compound that accumulates in acidified compartments. Upon lysosomal-PM fusion, the lysosomal pH would rapidly increase in addition to outward diffusion of the dye causing a loss of Lysotracker fluorescence intensity. **Figure 4E-H** shows that neither ER nor lysosomal membranes participate significantly in TMEM16F mediated exocytosis. In this connection, we have described previously similarly large Ca^{2+} activated membrane expansion in BHK fibroblasts. Ultrastructural analysis indicated that vesicular structures could not account for the membrane expansion, and the magnitudes of individual 'fusion' events were often equivalent to 100's of secretory vesicles (Wang and Hilgemann, 2008). Taken together, the previously reported large ‘fusion’ events and lack of a significant contribution from recycled endosomes, ER, and acidified lysosomes hint toward the involvement of membrane networks or other larger membrane structures in membrane expansion, as outlined in an accompanying article.

TMEM16F exocytosis and scrambling are followed by vesicle shedding.

Figures 5A and **5B** describe the relationships between cytoplasmic $Ca^{2+,}$ PS exposure, and membrane expansion during ionomycin exposure. **Figure 5A** illustrates concurrent imaging of cytoplasmic Ca^{2+} via the indicator, Fluo-4 (green), and PS exposure (red) via binding of a rhodamine labelled cationic peptide, heptalysine (K7r). We employed K7r, rather than AnnexinV, because it binds anionic phospholipids much faster and does not require Ca^{2+} for binding (Yaradanakul et al., 2008). Exposure to ionomycin (5 μM) results in very large increases of cytoplasmic Fluo-4 fluorescence followed by cell surface labelling of K7r, indicating large increases of cytoplasmic Ca^{2+} lead to externalization and exposure of PS. The full video of this experiment can be seen on **Figure 5-figure supplement 2**. **Figure 5B** illustrates parallel measurements of membrane expansion and phospholipid scrambling, monitored via C_m (red trace) and K7r (green trace), respectively. The two signals can be closely overlaid with one another during membrane expansion. Subsequent to membrane expansion and PS exposure, the two fluorescent signals decline in parallel. The fact that the K7r signal is not maintained on cells, as C_m declines, is indicative of the occurrence of extensive membrane shedding. This was readily visible in confocal microscopy and was typically preceded by the development of distinct membrane protrusions (**Figure 2-figure supplement 1**, **Figure 5-figure supplement 1 & 2**)

bioRxiv preprint doi: https://doi.org/10.1101/249227; this version posted January 16, 2018. The copyright holder for this preprint (which was not certified by peer review) is the author/funder. All rights reserved. No reuse allowed without permission.

In order to detect the fate of the shed membrane we treated wild-type and TMEM16F-null Jurkat T cells with Ca^{2+} ionophore for 10 minutes, then stained the cultures with Fluor®780 dye which binds to DNA. Flow cytometry was used to analyse subcellular-sized events (**Figure 5C**). All cultures contained similar levels of subcellular, DNA-containing particles. These are likely to be apoptotic bodies, as these cell cultures contain a small fraction of apoptotic cells (data not shown). However, Ca^{2+} ionophore treatment of WT but not TMEM16F-null Jurkat T cells resulted in a large increase of DNA-negative subcellular events, compatible with the release of numerous vesicles.

We next examined to what extent expression of TMEM16F and TMEM16F mutants, reported to have modified scrambling activity (Suzuki et al., 2010; Yang et al.), could rescue the TMEM16F-null phenotype. To do so, we employed the same CRISPR/Cas9 system to create a TMEM16F-null HEK 293 cell line that constitutively overexpresses the NCX1 Na/Ca exchanger (TMEM16F-null HEK-NCX cells), which can be used to generate transient Ca^{2+} elevations without ionomycin. As in Jurkat cells, Ca^{2+} influx in TMEM16F-null HEK293 cells caused rapid MEND (**Figure 5D**, red trace), and both membrane expansion (**Figure 5D**) and PS exposure (**Figure 5E**) could be restored by expressing mouse TMEM16F and its mutants. The D430G mutant has been reported to have constitutive PS scrambling activity (Suzuki et al., 2010). However, we found no clear difference between WT-rescue and D430G mutant-rescue in phospholipid scrambling similar to what has been described in more recent reports (Yang et al., 2012). Additionally we demonstrate no difference in membrane expansion for the D430G mutant vs WT rescue. Interestingly the Q559K mutant, which alters ion selectivity and slows activation kinetics (Yang et al., 2012) had both diminished PM scrambling and membrane expansion responses. However, the residual function of the Q559K mutant was adequate to prevent the MEND response seen in TMEM16F-null cells.

PD-1 traffics with Ca^{2+} -activated membrane movements.

To address the specificity of the large-scale trafficking events activated by Ca^{2+}, we next examined changes in the surface expression of T cell surface proteins via antibody staining. In WT Jurkat T cells there was a striking reduction in surface expression of the integral membrane protein PD-1 following Ca^{2+}-ionophore treatment (**Figure 6A**), compared to a number of other PM proteins. We used a PD-1/GFP fusion protein to demonstrate that this decrease in surface expression was due to loss of the molecule

bioRxiv preprint doi: https://doi.org/10.1101/249227; this version posted January 16, 2018. The copyright holder for this preprint (which was not certified by peer review) is the author/funder. All rights reserved. No reuse allowed without permission.

from the cells through membrane shedding, as both PD-1 surface staining and PD-1/GFP fluorescence were reduced upon ionophore treatment (**Figure 6B**). The extent of PD- 1/GFP loss was not as great as the loss of PD-1 surface staining (**Figure 6C**), as some of the PD-1/GFP is present intracellularily (data not shown, PD-1/mCherry shown in **Figure 6E**). Shed membrane containing antibody stained PD-1 and PD-1/GFP could be isolated from the supernatant of PD-1/GFP-expressing cells 15 minutes after ionomycin treatment (**Figure 6D**). Using a PD-1/mCherry fusion protein, we were able to resolve these PD-1 rich vesicles by Structured Illumination Microscopy (SR-SIM) (**Figure 6E**, **Figure 6-figure supplement 1**).

When we examined PD-1 surface expression in TMEM16F-null cells, detected by antibody staining, we found this also substantially decreased following Ca^{2+}- ionophore treatment (**Figure 6F**). In this case, however, the PD-1/GFP chimera was not lost from the cells when we quantitated GFP fluorescence after Ca^{2+}-stimulation (**Figure 6G-H**). Indeed, we could detect the PD-1/mCherry chimera in large intracellular vesicles (**Figure 6I**, **Figure 6-figure supplement 2**) demonstrating that it had been lost from the PM inwardly through the process of MEND. In order to examine which part of the PD-1 molecule controlled its trafficking, we constructed chimeras between PD-1 and HLA-A2, as HLA staining did not change in response to an increase in intracellular Ca^{2+} (**Figure 6A, F**). **Figure 6J** shows that the transmembrane domain of PD-1 targeted its sorting into shed membrane and MEND endosomes, in WT and TMEM16F null cells respectively.

bioRxiv preprint doi: https://doi.org/10.1101/249227; this version posted January 16, 2018. The copyright holder for this preprint (which was not certified by peer review) is the author/funder. All rights reserved. No reuse allowed without permission.

Discussion

Reconstitution experiments using a recombinant fungal TMEM16 in lipid vesicles demonstrate that this protein can function both as an ion channel and as a phospholipid scramblase that facilitated movement of phospholipids between the inner and outer monolayers of the surface membrane (Malvezzi et al.). Our results in intact cells show that TMEM16F also functions as a cytoplasmic Ca^{2+} sensor for large-scale membrane expansion that is followed by extensive membrane shedding. Deletion of TMEM16F blocks both scrambling and shedding and shifts this Ca^{2+} response from membrane expansion to massive endocytosis. Providing for the first time direct cellular evidence for why lipid scrambling many effect many of the diverse phenotypes demonstrated by this channel.

How are TMEM16F-induced membrane expansion, ion conduction and PS exposure related?

Membrane expansion occurs with nearly the same time course as TMEM16F conductance (**Figure 2A**) and are both blocked by cytoplasmic polyamines (**Figure 3**) a reagent known stop phospholipid scrambling in red blood cells. Furthermore, PS exposure and membrane expansion occur with very similar kinetics (**Figure 5B**), and both membrane expansion and scrambling are reduced by a mutation (Q559K) that affects the selectivity and activation kinetics of TMEM16F (**Figure 5D**). Together, these results suggest that the same Ca^{2+}-dependent conformational changes that activate TMEM16F conductance also trigger membrane expansion. One possibility is therefore that Ca^{2+}-stimulated phospholipid trafficking by TMEM16F is a trigger for membrane expansion. The appearance of specific phospholipids in the outer monolayer or the loss of specific lipid from the inner monolayer could be the trigger for membrane expansion. An alternative possibility is that activation of TMEM16F by Ca^{2+} activates large-scale exocytosis, and that PS exposure reflects fusion of vesicles that contain randomized phospholipids (Mirnikjoo et al., 2009; Lee et al., 2013). In an accompanying article we address the questions of whether membrane expansion in these experiments indeed reflects bona fide membrane fusion events and how TMEM16F activates membrane expansion.

How does TMEM16F prevent endocytosis?

bioRxiv preprint doi: https://doi.org/10.1101/249227; this version posted January 16, 2018. The copyright holder for this preprint (which was not certified by peer review) is the author/funder. All rights reserved. No reuse allowed without permission.

One of the most novel aspects presented is how the experiments outlined in this article clearly demonstrate that TMEM16F activity can determine whether membrane is added or removed from the PM in response to Ca^{2+} influx. Specifically, the occurrence of membrane expansion blocks the occurrence of endocytosis, presumably as a consequence of changing phospholipids in the surface membrane and/or changing the protein content of the membrane. The TMEM16F mutant Q559K, which has altered ion selectivity and slow activation kinetics (Yang et al., 2012), permits only a minimal amount of membrane expansion in response to Ca^{2+} influx, but it almost completely blocks endocytic responses. This suggests that a minimally active TMEM16F is sufficient to block endocytosis. It could be that TMEM16F prevents MEND by promoting membrane disorder. Alternatively, PS exposure, phospholipid scrambling and the presence of new membrane could alleviate lateral membrane tension during high intracellular Ca^{2+} events that would under those circumstances tend to vesiculate inward. Perhaps more likely, a new, multi-component signalling pathway with TMEM16F at the precipice controls rapid insertion and uptake of cellular membranes orders of magnitude larger than canonical SNARE mediated fusion and clathrin mediated endocytosis. These new pathways remain to be fully elucidated and are just now being brought to light.

Role of membrane traffic in membrane repair

It has long been recognised that cells can rapidly repair mechanical damage to their PM (Wilson, 1924). When the PM is damaged, for example by a physical lesion or a pore-forming toxin, the cytoplasmic Ca^{2+} concentration rises by up to 100-fold, leading to Ca^{2+}-dependent recruitment of endomembrane and membrane repair (Cooper and McNeil, 2015). This is one process that we are mimicking when induce a large increase of cytoplasmic Ca^{2+} using an ionophore. Physiological membrane damage and repair in animals have been most extensively studied in muscle (Cooper and McNeil, 2015) where mechanical damage induces Ca^{2+}-dependent membrane repair. Mutations in both dysferlin (Bansal et al., 2003) and TMEM16E (Griffin et al., 2016), which is closely related to TMEM16F and highly expressed in muscle, cause muscular dystrophies with limitations in membrane repair. Thus one potential function of Ca^{2+}-stimulated exocytosis dependent on TMEM16F may be membrane repair in some circumstances. Both exocytosis and endocytosis are suggested to have an involvement in membrane repair (Idone et al., 2008; Jimenez et al., 2014). Expression or activity of TMEM16F might therefore control the balance between these processes. The observation that the PD-1

bioRxiv preprint doi: https://doi.org/10.1101/249227; this version posted January 16, 2018. The copyright holder for this preprint (which was not certified by peer review) is the author/funder. All rights reserved. No reuse allowed without permission.

transmembrane region associates with membrane that is either shed or endocytosed depending on TMEM16F activity, suggests that particular membrane domains may be involved in Ca^{2+} stimulated trafficking.

Role of shed vesicles

There are also a number of possible functions of the vesicles which are shed following TMEM16F activation (**Figure 5, 6, Figure 5-figure supplement 1**). PS-expressing vesicles have been proposed to act as a catalyst for bone mineralization (Bevers and Williamson, 2016), and Scott syndrome (TMEM16F-null) cells do not produce these, because they do not expose PS (Bevers et al., 1992). This can explain why TMEM16F-null mice have defective embryonic bone formation (Ehlen et al., 2013). In T cells, we have detected vesicles shed from T cells containing the immune inhibitor PD-1, so vesicle shedding could be one mechanism by which PD-1 is down-regulated, preventing T cell exhaustion. Hu and colleagues (Hu et al., 2016) detected TMEM16F in endosomes that are recruited to the immunological synapse in T cells and postulated that PD-1 down-regulation was due to PD-1 endocytosis leading to degradation. However, our data suggest that recruitment of vesicles to the immune synapse followed by shedding of PD-1 is an intriguing and therapeutically important alternative possibility.

Vesicle shedding from T cells can be a localized phenomenon, for example following TCR triggering (Kumari et al., 2014). Our study is limited in that we have used a T cell line which is amenable to patch-clamp experiments, and a non-physiological Ca^{2+} ionophore stimulus to induce whole cell responses so that we can measure bulk plasma membrane changes using capacitance. Future studies of the role of TMEM16F measuring local vesicle shedding in primary T cells following receptor triggering are therefore warranted.

bioRxiv preprint doi: https://doi.org/10.1101/249227; this version posted January 16, 2018. The copyright holder for this preprint (which was not certified by peer review) is the author/funder. All rights reserved. No reuse allowed without permission.

Materials and Methods:

Data analysis was performed in Prism (GraphPad) or SigmaPlot (Systat) unless otherwise stated.

Cell lines, solutions and reagents

Jurkat E6.1 T cells (ECACC) were grown in RPMI-1640 (Sigma-Aldrich) while HEK-293 cells (Invitrogen) were grown in DMEM (Sigma-Aldrich). All media were supplemented with 10% FCS (Invitrogen), 2mM L-glutamine (Invitrogen) with 100 U/mL penicillin and 100 µg/mL streptomycin (Invitrogen). Standard cytoplasmic solution contained (in mM) 145 KCl, 10 HEPES, 0.5 EGTA, 0.25 $CaCl_2$, 8 MgATP, 2 TrisATP and 0.2 GTP, adjusted to pH 7.4. Extracellular 'Ringer' solution contained (in mM) 145 NaCl, 10 HEPES, 2 $CaCl_2$ and 2 $MgCl_2$, adjusted to pH 7. K^+-free *N*-Methyl-D-glucamine aspartate solution (NmAs) contained (in mM) 145 NMDG, 10 HEPES, and 0.5 EGTA, adjusted to pH 7 with aspartic acid; 2 $CaCl_2$ or 2 $MgCl_2$ were added when solution was used on the extracellular side while 0.25 and 0.5, resp., were used on the cytoplasmic side. Sucrose solution contained (in mM) 240 sucrose, 5 HEPES, 0.3 EGTA, and 5 KCl at pH 7; 2 $CaCl_2$ or 2 $MgCl_2$ were added when solution was used on the extracellular side while 0.25 and 0.5, resp., were used on the cytoplasmic side. 5µM ionomycin free acid (Calbiochem) was used unless otherwise stated. Other reagents used were: Lipofectamine 3000 (Life Technologies) for transient transfection protocols; STIM1-YFP (a generous gift Jen Liou, UTSW); 5µM FM 4-64 (Life Technologies), 400nM tetanus toxin L-chain (Alpha Universe LLC), 3µM latrunculin A (Sigma-Aldrich), 10µM phalloidin (Tocris), 3µM myristoylated dynamin inhibitory peptide (Tocris), 100nM LysoTracker Red DND-99 (Life Technologies), 50-500µM spermine (Sigma-Aldrich), and 100µg/ml (0.01%) Trypan Blue (Sigma-Aldrich). Rhodamine-conjugated hepta-lysine (rhodamine-KKKKKKK-amide; K7r) was prepared by Multiple Peptide Systems (NeoMPS, Inc.) and used at 3µM. Compared to Annexin V, K7r was advantageous for real-time imaging as membrane binding is significantly faster, and K7r binding does not require Ca^{2+}.

Whole-cell patch clamp with confocal imaging

Patch clamp recordings of cell electrical parameters were performed as described previously (Yaradanakul et al., 2008) using Capmeter v6.3 (Wang and Hilgemann, 2008) with National Instruments digital acquisition boards and Axopatch 200B or 1D patch clamp amplifiers. Square-wave voltage perturbation (20 mV; 0.5 kHz) was employed,

bioRxiv preprint doi: https://doi.org/10.1101/249227; this version posted January 16, 2018. The copyright holder for this preprint (which was not certified by peer review) is the author/funder. All rights reserved. No reuse allowed without permission.

input resistances were 2-9 MΩ, and the apparent cell resistances were 0.1-2 GΩ. External solutions were temperated to 35-37°C in parallel gravity-fed solution lines with outlet flow rates of 2 to 5mm/s. When confocal imaging and electrophysiology were combined, a Nikon TE2000-U microscope; 60× oil immersion, 1.45-NA objective paired with the EZ-C1confocal system (Nikon) containing a 40-mW 163-Argon laser (Spectra Physics; Newport Corporation) operating at 488 nm at 7.5% maximum capacity for FM4-64 and YFP recordings and a 1.5mW Melles Griot cylindrical HeNe laser at 543nm at 55% of maximum capacity for K7r, LysoTracker Red and Trypan Blue. Emission filters were set to either 500-540nm or 580LP. Typical resolution was 512 x 512, set with a pixel dwell time yielding <1-s exposure times per frame and a pinhole of 150µm. Image analysis was performed using either the EZ-C1 v3.9 (Nikon Instruments) or ImageJ (NIH). When imaging multiple fluorophores, sequential imaging was used to minimize spectral overlap. Photobleaching was negligible for these experiments. For independent confocal imaging of intact cells, 800µl of media containing Jurkat cells was transferred to a glass bottom 4-chamber dish. Warmed ionomycin solution was rapidly added at a 5:1 concentration and cells were imaged as described. For patch clamp, intracellular calcium stimulus was triggered by direct perfusion of the calcium ionophore ionomycin for Jurkat and HEK cell lines. HEK cells stably expressing the cardiac Na/Ca exchanger (NCX1.1) were stimulated through reverse transport by cytoplasmic pipette perfusion of cells with 40mM Na^+ and transient application of 2mM Ca^{2+} to the extracellular solution (Yaradanakul et al., 2008). No difference was detected in ionomycin or NXC induced stimulation of HEK cells (**Figure 5E**).

CRISPR-Cas9 knockdown of TMEM16F

The lentiCRISPR v2 plasmid was used as described (Sanjana et al., 2014). The guideRNA sequence targeting TMEM16F Exon 2 was 5'-TCAGCATGATTTTCGAACCC-3' and TMEM16F Exon 5 was 5'-TGTAAAAGTACACGCACCAT-3'. HEK-293 cells were transiently transfected with plasmid using Lipofectamine (Life Technologies) and the lentivirus was collected from the supernatant. Jurkat T cells and HEK-293 cells were transduced with lentivirus produced using the gag-pol expression vector p8.91 and VSV-G envelope vector pMDG as described previously (Zufferey et al., 1997). 48 hours after transduction cells were selected in 0.5µg/ml Puromycin for Jurkat and 5µg/ml Puromycin for HEK-293 before single-cell clones were isolated. Cells stably expressing Cas-9 and gRNA after transduction were frozen after initial expansion and aliquots thawed as

bioRxiv preprint doi: https://doi.org/10.1101/249227; this version posted January 16, 2018. The copyright holder for this preprint (which was not certified by peer review) is the author/funder. All rights reserved. No reuse allowed without permission.

needed to avoid accrued off-target effects resulting from long-term culture. Gene editing was confirmed by sequencing (Beckman Coulter) (**Figure 1-figure supplement 1**). Two different primer sets were used to amplify Exon 2 (Set 1 and 2) and one for Exon 5 (Set 3) and the amplicons sequenced using the same primers. Primer sequences were as follows (all 5' - 3'):

Set 1 FW GTGCAGGTTCATGCTTCATTT,
Set 1 RS GCACAGTCCCTGCAATAAGA,
Set 2 FW CCCGGTGCTGCTGATTTA,
Set 2 RS GGATCTACAGCCATTGAAGGAA,
Set 3 FW AGTGGTGGTCTCTGTATTGTTT ,
Set 3 RS AAACAGCAGGTTCCAAATTACC.

Proteomic analysis of Jurkat WT and CRISPR-Cas9 knock-out cells. Cells were subjected to Dounce homogenation on ice in 250 mM sucrose/10 mM Tris pH 7.4 with cOmplete protease inhibitor (Roche). Cell debris was pelleted and the supernatant was spun at 2000g for 60 min to pellet membrane. Membranes were washed and reconstituted with 4 X Laemmli buffer for SDS-PAGE. Protein bands were excised and digested overnight with trypsin (Pierce) following reduction and alkylation with DTT and iodoacetamide (Sigma-Aldrich). The samples underwent solid-phase extraction cleanup with Oasis HLB plates (Waters) and the resulting samples were analyzed by LC/MS/MS, using an Orbitrap Fusion Lumos mass spectrometer (Thermo Electron) coupled to an Ultimate 3000 RSLC-Nano liquid chromatography systems (Dionex). Raw MS data files were converted to a peak list format and analyzed using the central proteomics facilities pipeline (CPFP), version 2.0.3 (Trudgian et al., 2010; Trudgian and Mirzaei, 2012). Peptide identification was performed using the X!Tandem (Craig and Beavis, 2004) and open MS search algorithm (OMSSA) (Geer et al., 2004) search engines against the human protein database from Uniprot, with common contaminants and reversed decoy sequences appended (Elias and Gygi, 2007). Label-free quantitation of proteins across samples was performed using SINQ normalized spectral index Software (Trudgian et al., 2011).

Total Internal Reflection Fluorescence Microscopy (TIRFM)

Methods were adapted from (Zhang et al., 2007; Li et al., 2008). Jurkat T lymphocytes were incubated with 5μM FM4-64 in RPMI for 3 hours. Cells were then washed thoroughly and rested for 20 mins in Ringer solution before imaging in 8 well glass bottom μ-slides (1.5H, ibidi). Ionomycin was added to wells at a final concentration of

bioRxiv preprint doi: https://doi.org/10.1101/249227; this version posted January 16, 2018. The copyright holder for this preprint (which was not certified by peer review) is the author/funder. All rights reserved. No reuse allowed without permission.

5μM, 5s before recording began. Imaging was performed in an ElyraPS.1 inverted microscope (Zeiss), equipped with an EMCCD camera (iXon 897, Andor), in TIRF mode. Acquisition was done using a 100x TIRF objective (Plan-APOCHROMAT 100x/1.46 Oil, Zeiss), using the definite focus (Zeiss) to avoid drift in Z. The frame rate was 10fps. Putative fusion events were defined as complete puncta destaining to background level, with duration of destaining ≤1.5s (15 frames), with no sideways movement of puncta and were manually counted, while puncta number was quantified using QuickPALM (Henriques et al., 2010) and verified using ImageJ particle analysis after implementing Huang's fuzzy thresholding method using Shannon's entropy function and watershed algorithm (Huang, 1995).

Chimeric proteins, lentiviral vector constructs and production

All chimeric proteins were produced using overlap-extension PCR (Ho et al., 1989) and cloned into a single (pSIN) or dual (pDUAL) promoter vector. In fluorescent constructs a 'GS' linker separated PD-1 and fluorophore. Primers used to make PD1/GFP were PD1-FW, PD1GFP Sense, and PD1GFP Antisense GFP-RS. PD-1 mCherry was made in the same way using the primers PD1FW, PD1mCherry Sense, PD1mCherry Antisense and mCherry RS. PD1HLA Chimers were made with PD1-FW and HLA-A2-RS. For PD-1HLA-A2 chimeras, the extracellular portion was always PD-1 and the intracellular HLA-A2. The TM regions were the only sequences to vary between the two constructs. The transmembrane regions were predicted using the TMPred algorithm (https://embnet.vital-it.ch/software/TMPRED_form.html. The PD-1 TM was predicted as L168 to I191 and HLA-A2 TM I410 to W435. The chimera with PD-1 transmembrane was made with PD1TM Sense and PD1TM Antisense primers. The chimera with HLA-A2 transmembrane was made with HLATM Sense and HLATM Antisense primer. Lentivirus was produced using the gag-pol expression vector p8.91 and VSV-G envelope vector pMDG as described previously. The primer sequences were as follows:

PD1-FW GGGGGGATCCGCCACCATGCAGATCCCACAGGCGCC ,

PD1GFP Sense GGCTCCGGCTCCGGCTCCGTGAGCAAGGGCGAGGAGCT ,

PD1GFP Antisense GGAGCCGGAGCCGGAGCCGAGGGGCCAAGAGCAGTGTC ,

GFP-RS GCGGCCGCTTTACTTGTACAGCTCGTCCATGCCGAGAGTGATCCC ,

PD1mCherry Sense GGCTCCGGCTCCGGCTCCGTGAGCAAGGGCGAGGAGGA ,

PD1mCherry Antisense GACACTGCTCTTGGCCCCTCGGCTCCGGCTCCGGCTCC ,

mCherry RS GGCTCCGGCTCCGGCTCCGTGAGCAAGGGCGAGGAGGA ,

bioRxiv preprint doi: https://doi.org/10.1101/249227; this version posted January 16, 2018. The copyright holder for this preprint (which was not certified by peer review) is the author/funder. All rights reserved. No reuse allowed without permission.

HLA-A2-RS CCCCGCGGCCGCTCACACTTTACAAGCTGTGAGAGACACATCAG ,
PD1TM Sense TCTGGGTCCTGGCCGTCATCAGGAGGAAGAGCTCAGATAG ,
PD1TM Antisense CTATCTGAGCTCTTCCTCCTGATGACGGCCAGGACCCAGA ,
HLA TM Sense CAGCCGGCCAGTTCCAAACCATCGTGGGCATCATTGCTGG ,
HLA TM Antisense CCAGCAATGATGCCCACGATGGTTTGGAACTGGCCGGCTG.

Super-resolution structured illumination microscopy (SR-SIM) and Zeiss Airyscan microscopy

SR-SIM and Airyscan imaging was performed at 37°C using Plan-Apochromat 63x/1.4 oil DIC M27 objective in an Elyra PS.1 microscope (Zeiss). For SR-SIM, images were acquired using 5 phase shifts and 3 grid rotations, with 34µm grating period for the 561nm laser and filter set 4 (1851-248, Zeiss). Airyscan z-stacks were obtained at 0.75µm steps for a total depth of 12µm. Stacks were obtained every 30sec using a fast piezo controller and Definite Focus 2.0 (Zeiss) to avoid z-drift between time points. Processed images were projected into a single 2-D image based on maximum intensity using ImageJ. SR-SIM images were acquired using an sCMOS camera and high-resolution Airyscan images were acquired using the LS880 GaAsP detector, both processed using ZEN software (Zeiss).

Flow cytometry, antibodies and dyes

Cells were treated with ionomycin for 15min at 37°C in Ringer solution containing 2mM $CaCl_2$. Cells were stained for 30min on ice and flow cytometry was performed using a BD Fortessa (BD Bioscience). Intracellular Ca^{2+} concentration was monitored with 1µM Fluo-4 AM (Life Technologies) loaded in cells for 30min at 37°C prior to the experiment. Surface exposure of phosphatidylserine was detected using 9ng/ml Annexin V staining in Annexin binding buffer (BioLegend). Microvesicles were distinguished from apoptotic bodies using the DNA (Viability) eFluor® 780 dye (eBioscience). Surface staining for receptors was carried out for 30min on ice using the following antibodies: PD-1 APC (MIH4), ICAM-1 PE (HA58), Transferrin receptor (TfR) PE (M-A712) from BD Biosciences and CD28 PE (CD28.2), LFA-1 PE (HI111), CD4 PE (OKT4), CD3 PE/Cy7 (UCHT1), HLA ABC PE (W6/32) from BioLegend. Data were analyzed using FlowJo Software (Treestar).

bioRxiv preprint doi: https://doi.org/10.1101/249227; this version posted January 16, 2018. The copyright holder for this preprint (which was not certified by peer review) is the author/funder. All rights reserved. No reuse allowed without permission.

Figure Legends:

Figure 1. Fluo4-AM loaded WT and TMEM16F-null Jurkat T cells were treated with 5μM Ionomycin for 15 min, then stained with Annexin V and counted using fluorescence-activated cell sorting (FACS).

Figure 2. (A) Whole-cell patch clamp recordings indicating real-time measurements of membrane area (C_m) and transmembrane ion mobility (conductance) in WT Jurkat T cells with concurrent confocal imaging using standard Ringer and cytoplasmic solutions. FM4-64 (5μM) and ionomycin (5μM) were applied and washed as indicated. Single experimental traces with SEM values at 150 sec. post-stimulus display membrane area and FM4-64 fluorescence as a percentage of baseline values with confocal images at indicated time points. n=10. Scale bar is 5μm. **(B)** The same protocol as in (A) for TMEM16F-null Jurkat cells. n=10. **(C)** Percentage change in C_m 30s after ionomycin treatment of WT Jurkat cells. Cells were perfused with standard extracellular and cytoplasmic solutions plus indicated conditions for more than 200s before ionomycin treatment. Neither 400nM Tetanus Toxin L chain (TeNT) nor ATP/GTP exclusion (0 ATP) showed any significant effect on ionomycin stimulated C_m changes. (**$p \leq 0.01$) Isotonic replacement of most ions with sucrose blocked membrane expansion **(D)** Percentage change in C_m 30s after ionomycin treatment of TMEM16F-null Jurkat: Results are from left to right: KCl/NaCl solutions (Control), 3μM cytoplasmic dynamin inhibitory peptide, symmetrical K+-free NmAs solutions, symmetrical 3μM Latrunculin A, and 10μM cytoplasmic Phalloidin. (C, D represent mean values with SEM, n>7)

Figure 3. The polyamine, spermine, blocks membrane expansion and TMEM16F conductance with similar concentration dependencies. **(A)** Spermine at 250 and 500μM was added to cytoplasmic solutions. Cells were held for at least 300s before ionomycin treatment. Single experimental traces are given with mean C_m change and SEM. n>7. **(B)** Change in membrane area (ΔC_m in %) and peak G_m magnitudes were determined during ionomycin application. C_m and G_m responses were compared to control responses without spermine (* $p \leq 0.05$, ** $p \leq 0.01$, ***$p \leq 0.001$ ****$p \leq 0.0001$).

Figure 4. (A-B) Multi-Dimensional Super Resolution Airyscan Microscopy. **(A)** Representative pictographs illustrating FM-labelled punctae in WT Jurkat cells before and 5 min after ionomycin treatment. Jurkat cells were attached to fibronectin-coated imaging plates and standard ringer was supplemented with ionomycin after imaging was stabilized for a minimum of 4 frames. 30s frame times **(B)** Quantification of projected

bioRxiv preprint doi: https://doi.org/10.1101/249227; this version posted January 16, 2018. The copyright holder for this preprint (which was not certified by peer review) is the author/funder. All rights reserved. No reuse allowed without permission.

0.75 µm z-stacks reveals no significant change to the number of punctae before and after treatment. n=5 independent experiments. **(C-D)** TIRF microscopy captures the Ca^{2+} activated disappearance of FM-labelled puncta in WT but not TMEM16F-null Jurkat T cells following ionomycin treatment. As in **(A-B)** however cells were supplemented with ionomycin 5s before imaging. Values are expressed as a percentage of the initial average number of puncta calculated at 0, 5 and 10 secs. **(E-F)** Attached HEK TMEM16F-null and mTMEM16F-rescue cells transiently expressing the ER membrane protein STIM1 containing a luminal (ER-resident) YFP fluorophore (Liou et al., 2005) were imaged with extracellular application of 100 µg/ml TB to transiently quench extracellular fluorescence of YFP. Cells were exposed to 5µM ionomycin to stimulate membrane fusion. Exposure of the luminal YFP domain of STIM1 during membrane expansion would allow for increased quenching of fluorescence by extracellular TB. No significant change in fluorescence was detected. Analysis shows percentage of initial YFP fluorescence prior to and 300 s after ionomycin stimulation. n=5. Mean values and SEM depicted. **(G-H)** Newly expanded membrane is not associated with lysosomal probes. TMEM16F expressing and TMEM16F-null cells were stained for 60min with 100nM of LysoTracker Red. The probe is highly selective for acidic organelles and accumulates in lysosomal compartments. Cells were imaged before and after buffer was supplemented with 5µM ionomycin and 2mM Ca^{2+}. Lysosomal fusion to the PM would result in release of fluorescent cargo and loss of labelling. Analysis reveals no detectible loss of fluorescent punctae across both cell lines using ImageJ (NIH) to determine average fluorescence value per cell area with SEM before and after ionomycin stimulation. n=10.

Figure 5. (A) Pictograph of Fluo4 and Polylysine-rhodamine (K7r) labelled WT Jurkat cells indicating mean increase and median time to maximal increase for both Ca^{2+} and K7r PS binding. n=4 **(B)** Real-time membrane scrambling and C_m were measured with K7r membrane binding with concurrent whole-cell patch-clamp of WT Jurkat T cells using standard solutions following ionomycin treatment. Images are of K7r binding to the cell at indicated time points with scale bar representing 10µm. Experimental traces from this cell are shown. **(C)** WT Jurkat T cells were treated for 15 min with ionomycin in Ringer and stained with DNA (Viability) eFluor®780 dye (eBioscience). Subcellular sized events were gated and apoptotic bodies distinguished from microvesicles by DNA dye uptake. Numbers are percentage of total events. **(D)** HEK 293 TMEM16F-null cells transfected with WT, D409G or Q559K mouse TMEM16F. Cells were imaged before and

bioRxiv preprint doi: https://doi.org/10.1101/249227; this version posted January 16, 2018. The copyright holder for this preprint (which was not certified by peer review) is the author/funder. All rights reserved. No reuse allowed without permission.

after Ca^{2+} transients (NCX1 reverse exchange or ionomycin when indicated), and the percentage change in C_m was calculated for each group. (**p ≤ 0.01) Single recordings displayed with mean values and SEM at 30, 45 and 60s after stimulus Mean values with SEM of n>7. **(E)** Fold change in K7r binding for cells described in (D). n>7 for each group

Figure 6. (A) WT Jurkat T cells expressing PD-1 were treated with ionomycin for 15 mins in Ringer solution and stained for expression of surface molecules. Data are percentage of initial surface expression following ionomycin treatment. **(B)** and **(C)** PD1/GFP chimera was expressed on WT Jurkat T cells. Surface PD-1 and total GFP with and without ionomycin treatment are shown. **(D)** Jurkat WT control and WT PD-1/GFP chimera expressing cells were stimulated with ionomycin. Vesicles were gated for as subcellular sized events with low DNA dye uptake. PD-1 and GFP expression on shed vesicles is shown. **(E)** PD1-mCherry chimera was expressed in WT Jurkat T cells and imaged by SR-SIM microscopy before and after ionomycin treatment. Arrows indicate PD1-bearing microvesicles. **(F)** TMEM16F-null cells were treated and stained as in (**A**). **(G)** and **(H)**, PD1GFP chimera was expressed in TMEM16F-null Jurkat T cells. Surface PD-1 and total GFP with and without ionomycin treatment are shown. **(I)**, PD1-mCherry chimera was expressed in TMEM16F-null Jurkat T cells and imaged by SR-SIM microscopy before and after ionomycin treatment. **(J)**, PD1HLA-A2 chimeras were produced and expressed in WT and TMEM16F-null Jurkat T cells. Percentage surface expression remaining after treatment with ionomycin is shown. (**p ≤ 0.01, ***p ≤ 0.001 ****p ≤ 0.0001). (For E and I, scale bar is 5 µm; For A, C, F, H, K For A, C, F, H, K, FACS data is for three independent repeats employing >10,000 cells per condition. Data points give mean values with SEM.

bioRxiv preprint doi: https://doi.org/10.1101/249227; this version posted January 16, 2018. The copyright holder for this preprint (which was not certified by peer review) is the author/funder. All rights reserved. No reuse allowed without permission.

Supplementary Figure Legends:

Figure 1 - figure supplement 1. (A) TMEM16F was edited using the lentiviral vector-based CRISPR-Cas9 system. Cells were verified genomically using sequencing analysis and functionally assayed for PS exposure with Annexin V as described in **Figure 4A**. TMEM16F Exon 2 and target sequence is shown. (B) Two sets of primers were used to amplify TMEM16F Exon 2 from vector-only transduced Jurkat T cell genomic DNA. The two amplicons were then sequenced. (C) The same amplicons were sequenced from a clone transduced with TMEM16F Exon 2-targeted CRISPR-Cas9 lentiviral vector. (D) The result of the single nucleotide insertion on the amino acid sequence. A stop codon results 10 nucleotides downstream of the insertion that truncates TMEM16F from 910 to 50 amino acids. (E) TMEM16F Exon 5 and target sequence. (F) One primer set was used to amplify TMEM16F Exon 5 from vector-only transduced Jurkat T cell genomic DNA and sequenced (G) The same amplicon was sequenced from a clone transduced with TMEM16F Exon 5-targeted CRISPR-Cas9 lentiviral vector. The indeterminate sequence 3' of the target sequence is suggestive of differently mutated alleles and was consistent across repeats. (H) WT, TMEM16F-null cells CRISPR-targeted to either Exon 2 or Exon 5 were treated with 5μM ionomycin for 15 min or 2μM Etoposide overnight and stained with Annexin V and compared to untreated cells. WT cells treated with ionomycin show a clear increase in Annexin V binding to exposed phosphatidylserine. Both Exon2 and Exon 5 TMEM16F-null cell lines fail to show Annexin V binding responses during ionomycin treatments, demonstrating that ionomycin-induced scrambling is consistently blocked in cell lines where TMEM16F was targeted for CRISPR-Cas9 excision. Loss of TMEM16F does not interfere with apoptosis-induced scrambling and PS exposure as overnight treatment of Etoposide shows similar increases in Annexin V positive cells for WT and both Exon2 and Exon5 targeted cell lines. Exon2 targeted cell lines were used for further experiments.

Figure 1 – figure supplement 2. Proteomics analysis of Jurkat WT and CRISPR-Cas9 TMEM16F-null cells. Table describing surface proteins and TMEM16F expression in parental and stably selected Jurkat cell lines.

Figure 2 – figure supplement 1 (video). Ca^{2+}-induced exocytosis and shedding probed with FM4-64 in WT Jurkat T cells. WT Jurkat cells were plated in a chambered coverslip

bioRxiv preprint doi: https://doi.org/10.1101/249227; this version posted January 16, 2018. The copyright holder for this preprint (which was not certified by peer review) is the author/funder. All rights reserved. No reuse allowed without permission.

in Ringer with 5μM FM 4-64. 5μM ionomycin was added at 30s. The scale bar represents 10μm.

Figure 2 – figure supplement 2. SR-SIM microscopy images of FM4-64 dye distribution before **(A)** and after **(B)** Ca^{2+} influx in TMEM16F-null Jurkat T cells. **(C)** and **(D)** show the time course of MEND in two regions of interest (blue (C) and green (D)). Intracellular vesicles decorated with FM4-64 are visible following MEND, with no evidence of PM permeabilization to FM4-64. The scale bars represent 10 μm.

Figure 5 – figure supplement 1 (video). Ca^{2+}induced PS exposure probed with K7r in WT Jurkat T cells. WT Jurkat cells were plated in a chambered coverslip in Ringer with 3μM K7r. 5 μM ionomycin was added at 50s. The scale bar represents 10μm.

Figure 5 – figure supplement 2 (video). Similar to Figure 5 Supplemental 1 Video corresponding the experiment quantified in Figure 5A. Ca^{2+}induced PS exposure probed with K7r in WT Jurkat T cells. WT Jurkat cells were pre-incubated with 3μM Fluo-4 (green) and plated in a chambered coverslip in Ringer with 3μM K7r (red). 5 μM ionomycin was added at 80s. The scale bar represents 10μm.

Figure 6 – figure supplement 1 (video). In WT Jurkat T cells PD-1 is shed following ionomycin treatment. PD1- mCherry expressing WT Jurkat T cells were imaged by SR-SIM Microscopy. Ionomycin was added to the opposite side of the chambered cover slip 10s before the video starts. Scale bar represents 10 μm.

Figure 6 – figure supplement 2 (video). In TMEM16F-null Jurkat T cells PD-1 is endocytosed following ionomycin treatment. PD1-mCherry expressing TMEM16F-null Jurkat T cells were imaged by SR-SIM Microscopy. Ionomycin was added to the opposite side of the chambered cover slip 10s before the video starts. Scale bar represents 10μm.

bioRxiv preprint doi: https://doi.org/10.1101/249227; this version posted January 16, 2018. The copyright holder for this preprint (which was not certified by peer review) is the author/funder. All rights reserved. No reuse allowed without permission.

Reference List

Anderson, H.C. 2003. Matrix vesicles and calcification. *Curr Rheumatol Rep*. 5:222-226.

Bansal, D., K. Miyake, S.S. Vogel, S. Groh, C.C. Chen, R. Williamson, P.L. McNeil, and K.P. Campbell. 2003. Defective membrane repair in dysferlin-deficient muscular dystrophy. *Nature*. 423:168-172. doi:10.1038/nature01573.

Batti, L., M. Sundukova, E. Murana, S. Pimpinella, F. De Castro Reis, F. Pagani, H. Wang, E. Pellegrino, E. Perlas, S. Di Angelantonio, D. Ragozzino, and P.A. Heppenstall. 2016. TMEM16F Regulates Spinal Microglial Function in Neuropathic Pain States. *Cell Rep*. 15:2608-2615. doi:10.1016/j.celrep.2016.05.039.

Bevers, E.M., T. Wiedmer, P. Comfurius, S.J. Shattil, H.J. Weiss, R.F. Zwaal, and P.J. Sims. 1992. Defective Ca(2+)-induced microvesiculation and deficient expression of procoagulant activity in erythrocytes from a patient with a bleeding disorder: a study of the red blood cells of Scott syndrome. *Blood*. 79:380-388.

Bevers, E.M., and P.L. Williamson. 2010. Phospholipid scramblase: an update. *FEBS Lett*. 584:2724-2730. doi:10.1016/j.febslet.2010.03.020.

Bevers, E.M., and P.L. Williamson. 2016. Getting to the Outer Leaflet: Physiology of Phosphatidylserine Exposure at the Plasma Membrane. *Physiological reviews*. 96:605-645. doi:10.1152/physrev.00020.2015.

Bratton, D.L. 1994. Polyamine inhibition of transbilayer movement of plasma membrane phospholipids in the erythrocyte ghost. *J Biol Chem*. 269:22517-22523.

Brunner, J.D., N.K. Lim, S. Schenck, A. Duerst, and R. Dutzler. 2014. X-ray structure of a calcium-activated TMEM16 lipid scramblase. *Nature*. 516:207-212. doi:10.1038/nature13984.

Cooper, S.T., and P.L. McNeil. 2015. Membrane Repair: Mechanisms and Pathophysiology. *Physiological reviews*. 95:1205-1240. doi:10.1152/physrev.00037.2014.

Craig, R., and R.C. Beavis. 2004. TANDEM: matching proteins with tandem mass spectra. *Bioinformatics (Oxford, England)*. 20:1466-1467. doi:10.1093/bioinformatics/bth092.

Ehlen, H.W.A., M. Chinenkova, M. Moser, H.-M. Munter, Y. Krause, S. Gross, B. Brachvogel, M. Wuelling, U. Kornak, and A. Vortkamp. 2013. Inactivation of anoctamin-6/Tmem16f, a regulator of phosphatidylserine scrambling in osteoblasts, leads to decreased mineral deposition in skeletal tissues. *J. Bone Miner. Res.* 28:246-259. doi:papers3://publication/doi/10.1002/jbmr.1751.

Elias, J.E., and S.P. Gygi. 2007. Target-decoy search strategy for increased confidence in large-scale protein identifications by mass spectrometry. *Nature methods*. 4:207-214. doi:10.1038/nmeth1019.

Griffin, D.A., R.W. Johnson, J.M. Whitlock, E.R. Pozsgai, K.N. Heller, W.E. Grose, W.D. Arnold, Z. Sahenk, H.C. Hartzell, and L.R. Rodino-Klapac. 2016. Defective membrane fusion and repair in Anoctamin5-deficient muscular dystrophy. *Human molecular genetics*. 25:1900-1911. doi:10.1093/hmg/ddw063.

Gyobu, S., H. Miyata, M. Ikawa, D. Yamazaki, H. Takeshima, J. Suzuki, and S. Nagata. 2015. A Role of TMEM16E Carrying a Scrambling Domain in Sperm Motility. *Mol Cell Biol*. 36:645-659. doi:10.1128/MCB.00919-15.

Headland, S.E., H.R. Jones, L.V. Norling, A. Kim, P.R. Souza, E. Corsiero, C.D. Gil, A. Nerviani, F. Dell'Accio, C. Pitzalis, S.M. Oliani, L.Y. Jan, and M. Perretti. 2015. Neutrophil-derived microvesicles enter cartilage and protect the joint in inflammatory arthritis. *Sci Transl Med*. 7:315ra190. doi:10.1126/scitranslmed.aac5608.

bioRxiv preprint doi: https://doi.org/10.1101/249227; this version posted January 16, 2018. The copyright holder for this preprint (which was not certified by peer review) is the author/funder. All rights reserved. No reuse allowed without permission.

Henriques, R., M. Lelek, E.F. Fornasiero, F. Valtorta, C. Zimmer, and M.M. Mhlanga. 2010. QuickPALM: 3D real-time photoactivation nanoscopy image processing in ImageJ. *Nature methods*. 7:339-340. doi:10.1038/nmeth0510-339.

Ho, S.N., H.D. Hunt, R.M. Horton, J.K. Pullen, and L.R. Pease. 1989. Site-directed mutagenesis by overlap extension using the polymerase chain reaction. *Gene*. 77:51-59.

Hu, Y., J.H. Kim, K. He, Q. Wan, J. Kim, M. Flach, T. Kirchhausen, A. Vortkamp, and F. Winau. 2016. Scramblase TMEM16F terminates T cell receptor signaling to restrict T cell exhaustion. *J Exp Med*. 213:2759-2772. doi:10.1084/jem.20160612.

Huang, L.K.W., M.J. 1995. Image thresholding by minimizing the measure of fuzziness. *Pattern Recognition*. 28:41-51.

Idone, V., C. Tam, J.W. Goss, D. Toomre, M. Pypaert, and N.W. Andrews. 2008. Repair of injured plasma membrane by rapid Ca2+-dependent endocytosis. *J Cell Biol*. 180:905-914. doi:jcb.200708010 [pii]

10.1083/jcb.200708010 [doi].

Jimenez, A.J., P. Maiuri, J. Lafaurie-Janvore, S. Divoux, M. Piel, and F. Perez. 2014. ESCRT machinery is required for plasma membrane repair. *Science*. 343:1247136. doi:10.1126/science.1247136.

Kumari, S., S. Curado, V. Mayya, and M.L. Dustin. 2014. T cell antigen receptor activation and actin cytoskeleton remodeling. *Biochim Biophys Acta*. 1838:546-556. doi:10.1016/j.bbamem.2013.05.004.

Lariccia, V., M. Fine, S. Magi, M.-J. Lin, A. Yaradanakul, M.C. Llaguno, and D.W. Hilgemann. 2011. Massive calcium-activated endocytosis without involvement of classical endocytic proteins. *J. Gen. Physiol.* 137:111-132. doi:papers3://publication/doi/10.1085/jgp.201010468.

Lee, S.H., X.W. Meng, K.S. Flatten, D.A. Loegering, and S.H. Kaufmann. 2013. Phosphatidylserine exposure during apoptosis reflects bidirectional trafficking between plasma membrane and cytoplasm. *Cell Death Differ*. 20:64-76. doi:10.1038/cdd.2012.93.

Leventis, P.A., and S. Grinstein. 2010. The distribution and function of phosphatidylserine in cellular membranes. *Annual review of biophysics*. 39:407-427. doi:10.1146/annurev.biophys.093008.131234.

Li, D., N. Ropert, A. Koulakoff, C. Giaume, and M. Oheim. 2008. Lysosomes are the major vesicular compartment undergoing Ca2+-regulated exocytosis from cortical astrocytes. *J Neurosci*. 28:7648-7658. doi:10.1523/JNEUROSCI.0744-08.2008.

Liou, J., M.L. Kim, W.D. Heo, J.T. Jones, J.W. Myers, J.E. Ferrell, Jr., and T. Meyer. 2005. STIM is a Ca2+ sensor essential for Ca2+-store-depletion-triggered Ca2+ influx. *Current biology : CB*. 15:1235-1241. doi:10.1016/j.cub.2005.05.055.

Malvezzi, M., M. Chalat, R. Janjusevic, A. Picollo, H. Terashima, A.K. Menon, and A. Accardi. 2013. Ca2+-dependent phospholipid scrambling by a reconstituted TMEM16 ion channel. *Nat Commun*. 4:2367. doi:10.1038/ncomms3367.

Marino, G., and G. Kroemer. 2013. Mechanisms of apoptotic phosphatidylserine exposure. *Cell research*. 23:1247-1248. doi:10.1038/cr.2013.115.

Matti, U., V. Pattu, M. Halimani, C. Schirra, E. Krause, Y. Liu, L. Weins, H.F. Chang, R. Guzman, J. Olausson, M. Freichel, F. Schmitz, M. Pasche, U. Becherer, D. Bruns, and J. Rettig. 2013. Synaptobrevin2 is the v-SNARE required for cytotoxic T-lymphocyte lytic granule fusion. *Nat Commun*. 4:1439. doi:10.1038/ncomms2467.

Mirnikjoo, B., K. Balasubramanian, and A.J. Schroit. 2009. Suicidal Membrane Repair Regulates Phosphatidylserine Externalization during Apoptosis. *J. Biol. Chem.* 284:22512-22516. doi:papers3://publication/doi/10.1074/jbc.C109.022913.

bioRxiv preprint doi: https://doi.org/10.1101/249227; this version posted January 16, 2018. The copyright holder for this preprint (which was not certified by peer review) is the author/funder. All rights reserved. No reuse allowed without permission.

Ousingsawat, J., P. Wanitchakool, A. Kmit, A.M. Romao, W. Jantarajit, R. Schreiber, and K. Kunzelmann. 2015a. Anoctamin 6 mediates effects essential for innate immunity downstream of P2X7 receptors in macrophages. *Nat Comms*. 6:6245-6245. doi:papers3://publication/doi/10.1038/ncomms7245.

Ousingsawat, J., P. Wanitchakool, R. Schreiber, M. Wuelling, A. Vortkamp, and K. Kunzelmann. 2015b. Anoctamin-6 controls bone mineralization by activating the calcium transporter NCX1. *Journal of Biological Chemistry*. 290:6270-6280. doi:papers3://publication/doi/10.1074/jbc.M114.602979.

Pardoll, D.M. 2012. The blockade of immune checkpoints in cancer immunotherapy. *Nat. Rev. Cancer*. 12:252-264. doi:papers3://publication/doi/doi:10.1038/nrc3239

10.1038/nrc3239.

Reddy, A., E.V. Caler, and N.W. Andrews. 2001. Plasma membrane repair is mediated by Ca(2+)-regulated exocytosis of lysosomes. *Cell*. 106:157-169.

Sanjana, N.E., O. Shalem, and F. Zhang. 2014. Improved vectors and genome-wide libraries for CRISPR screening. *Nature methods*. 11:783-784. doi:10.1038/nmeth.3047.

Schreiber, R., I. Uliyakina, P. Kongsuphol, R. Warth, M. Mirza, J.R. Martins, and K. Kunzelmann. 2010. Expression and function of epithelial anoctamins. *J Biol Chem*. 285:7838-7845. doi:10.1074/jbc.M109.065367.

Suzuki, J., M. Umeda, P.J. Sims, and S. Nagata. 2010. Calcium-dependent phospholipid scrambling by TMEM16F. *Nature*. 468:834-838. doi:papers3://publication/doi/10.1038/nature09583.

Trudgian, D.C., and H. Mirzaei. 2012. Cloud CPFP: a shotgun proteomics data analysis pipeline using cloud and high performance computing. *Journal of proteome research*. 11:6282-6290. doi:10.1021/pr300694b.

Trudgian, D.C., G. Ridlova, R. Fischer, M.M. Mackeen, N. Ternette, O. Acuto, B.M. Kessler, and B. Thomas. 2011. Comparative evaluation of label-free SINQ normalized spectral index quantitation in the central proteomics facilities pipeline. *Proteomics*. 11:2790-2797. doi:10.1002/pmic.201000800.

Trudgian, D.C., B. Thomas, S.J. McGowan, B.M. Kessler, M. Salek, and O. Acuto. 2010. CPFP: a central proteomics facilities pipeline. *Bioinformatics (Oxford, England)*. 26:1131-1132. doi:10.1093/bioinformatics/btq081.

Wan, C.P., C.S. Park, and B.H. Lau. 1993. A rapid and simple microfluorometric phagocytosis assay. *Journal of immunological methods*. 162:1-7.

Wang, T.M., and D.W. Hilgemann. 2008. Ca-dependent nonsecretory vesicle fusion in a secretory cell. *The Journal of general physiology*. 132:51-65. doi:10.1085/jgp.200709950.

Wilson, E.B. 1924. The Cell in Development and Heredity. New York: Macmillan.

Yang, H., A. Kim, T. David, D. Palmer, T. Jin, J. Tien, F. Huang, T. Cheng, S.R. Coughlin, Y.N. Jan, and L.Y. Jan. 2012. TMEM16F forms a Ca2+-activated cation channel required for lipid scrambling in platelets during blood coagulation. *Cell*. 151:111-122. doi:10.1016/j.cell.2012.07.036.

Yaradanakul, A., T.M. Wang, V. Lariccia, M.J. Lin, C. Shen, X. Liu, and D.W. Hilgemann. 2008. Massive Ca-induced membrane fusion and phospholipid changes triggered by reverse Na/Ca exchange in BHK fibroblasts. *The Journal of general physiology*. 132:29-50. doi:10.1085/jgp.200709865.

Yu, K., J.M. Whitlock, K. Lee, E.A. Ortlund, Y.Y. Cui, and H.C. Hartzell. 2015. Identification of a lipid scrambling domain in ANO6/TMEM16F. *Elife*. 4:e06901. doi:10.7554/eLife.06901.

bioRxiv preprint doi: https://doi.org/10.1101/249227; this version posted January 16, 2018. The copyright holder for this preprint (which was not certified by peer review) is the author/funder. All rights reserved. No reuse allowed without permission.

Zhang, Z., G. Chen, W. Zhou, A. Song, T. Xu, Q. Luo, W. Wang, X.S. Gu, and S. Duan. 2007. Regulated ATP release from astrocytes through lysosome exocytosis. *Nat Cell Biol*. 9:945-953. doi:10.1038/ncb1620.

Zufferey, R., D. Nagy, R.J. Mandel, L. Naldini, and D. Trono. 1997. Multiply attenuated lentiviral vector achieves efficient gene delivery in vivo. *Nature biotechnology*. 15:871-875. doi:10.1038/nbt0997-871.

bioRxiv preprint doi: https://doi.org/10.1101/249227; this version posted January 16, 2018. The copyright holder for this preprint (which was not certified by peer review) is the author/funder. All rights reserved. No reuse allowed without permission.

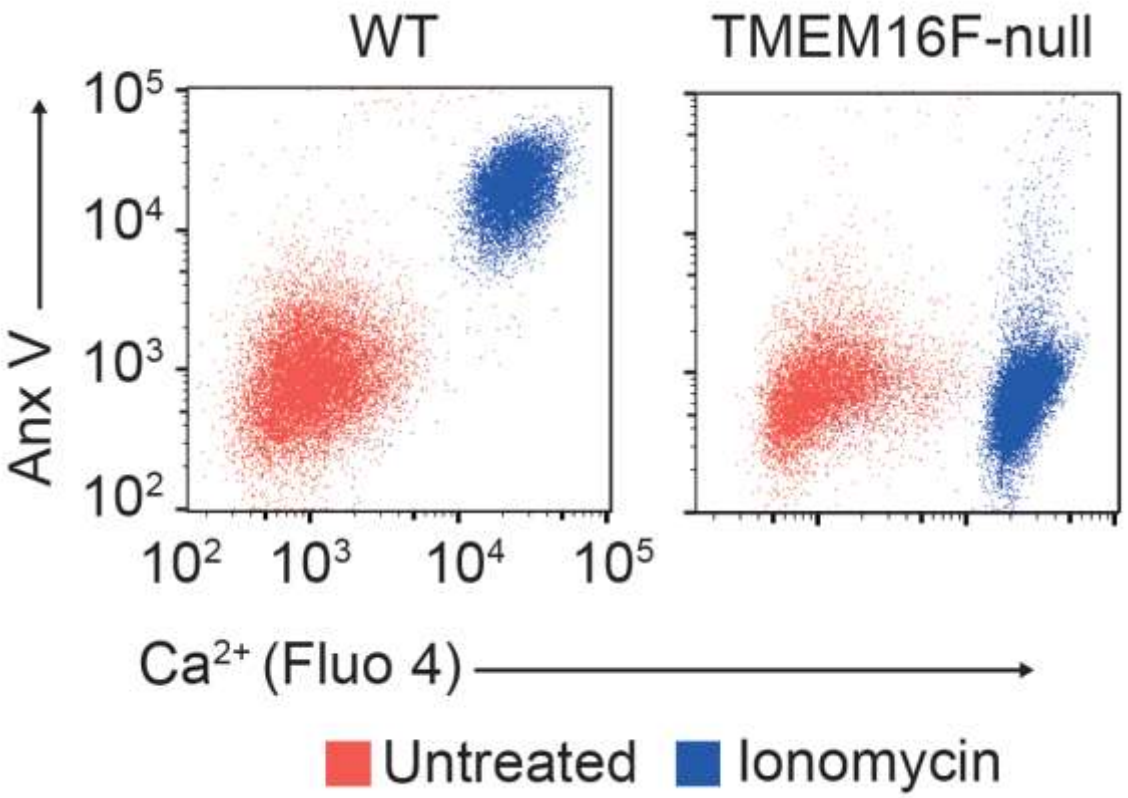

Figure 1

bioRxiv preprint doi: https://doi.org/10.1101/249227; this version posted January 16, 2018. The copyright holder for this preprint (which was not certified by peer review) is the author/funder. All rights reserved. No reuse allowed without permission.

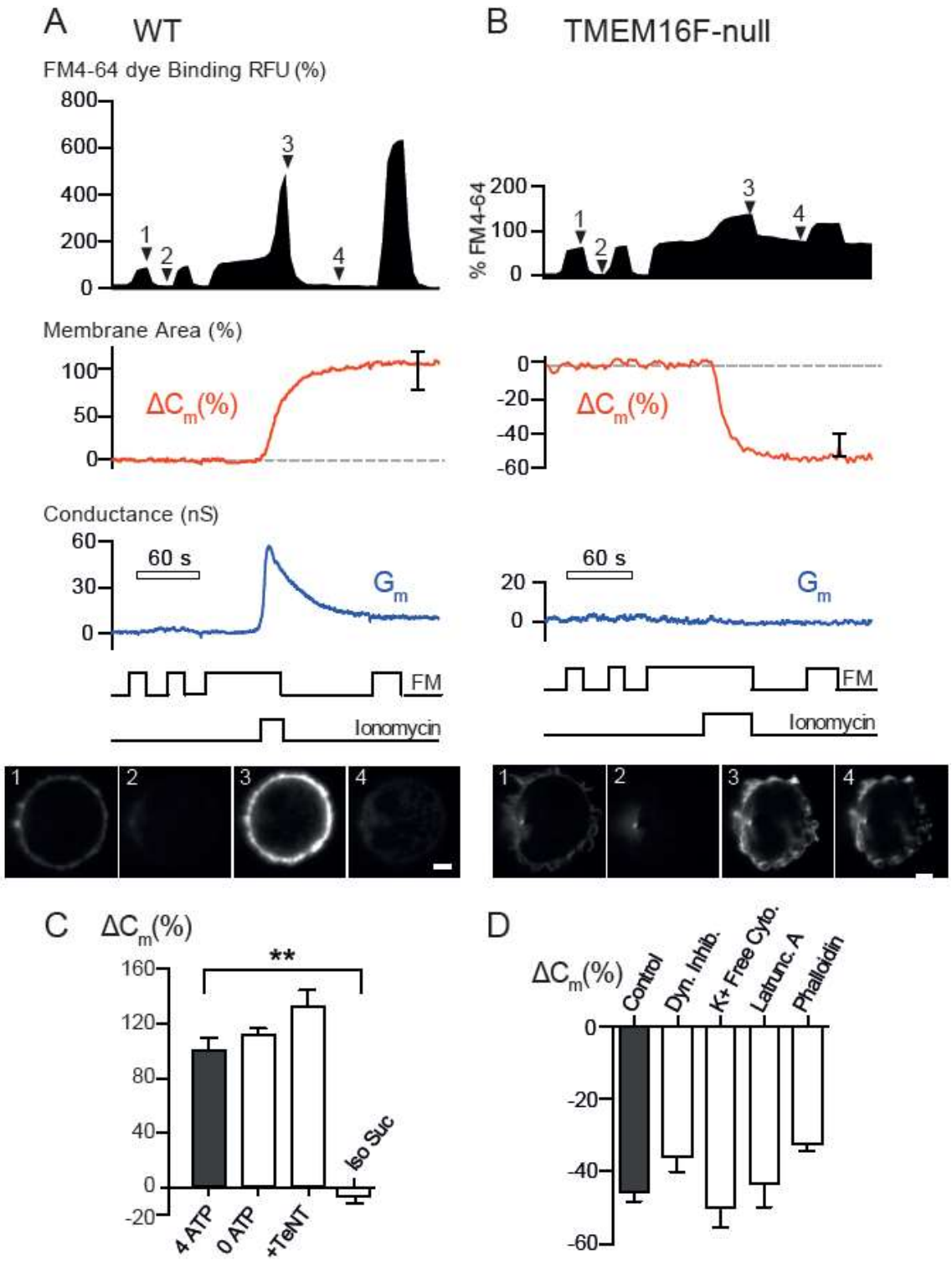

Figure 2

bioRxiv preprint doi: https://doi.org/10.1101/249227; this version posted January 16, 2018. The copyright holder for this preprint (which was not certified by peer review) is the author/funder. All rights reserved. No reuse allowed without permission.

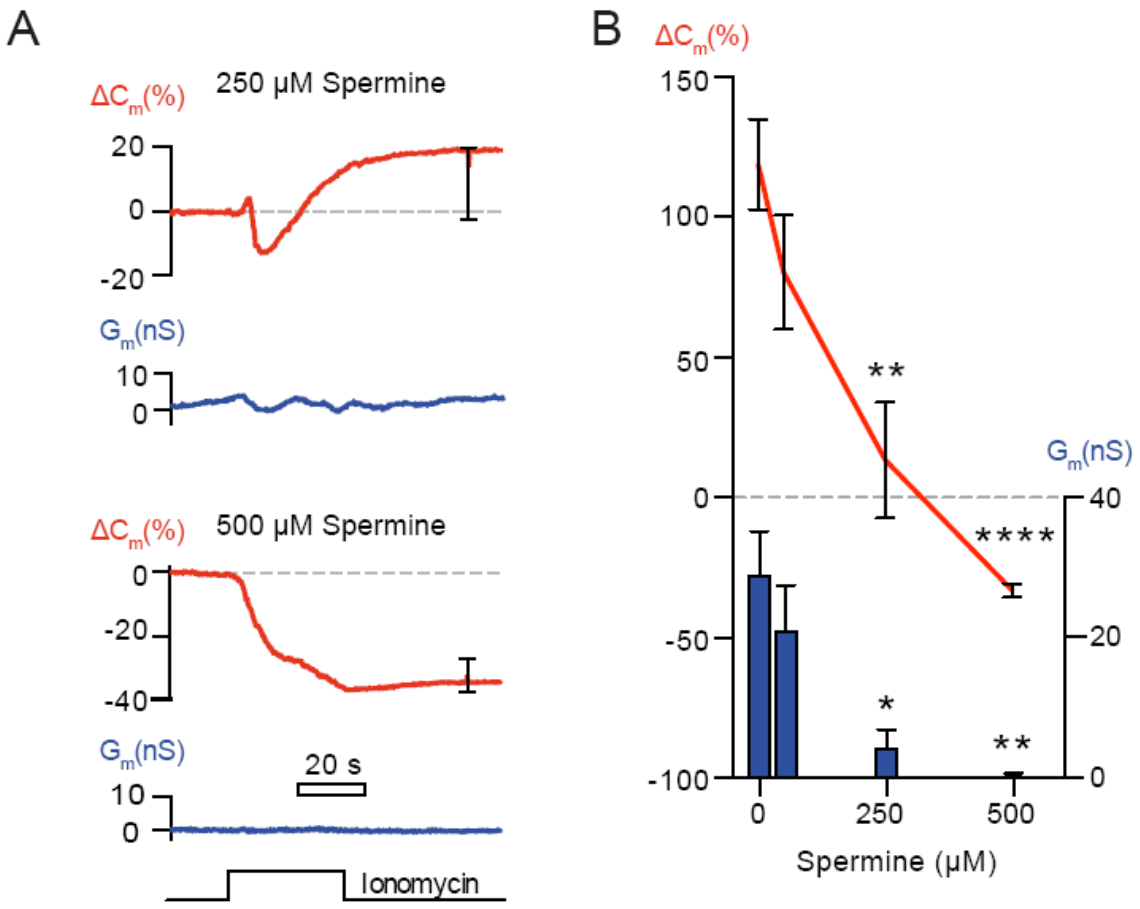

Figure 3

bioRxiv preprint doi: https://doi.org/10.1101/249227; this version posted January 16, 2018. The copyright holder for this preprint (which was not certified by peer review) is the author/funder. All rights reserved. No reuse allowed without permission.

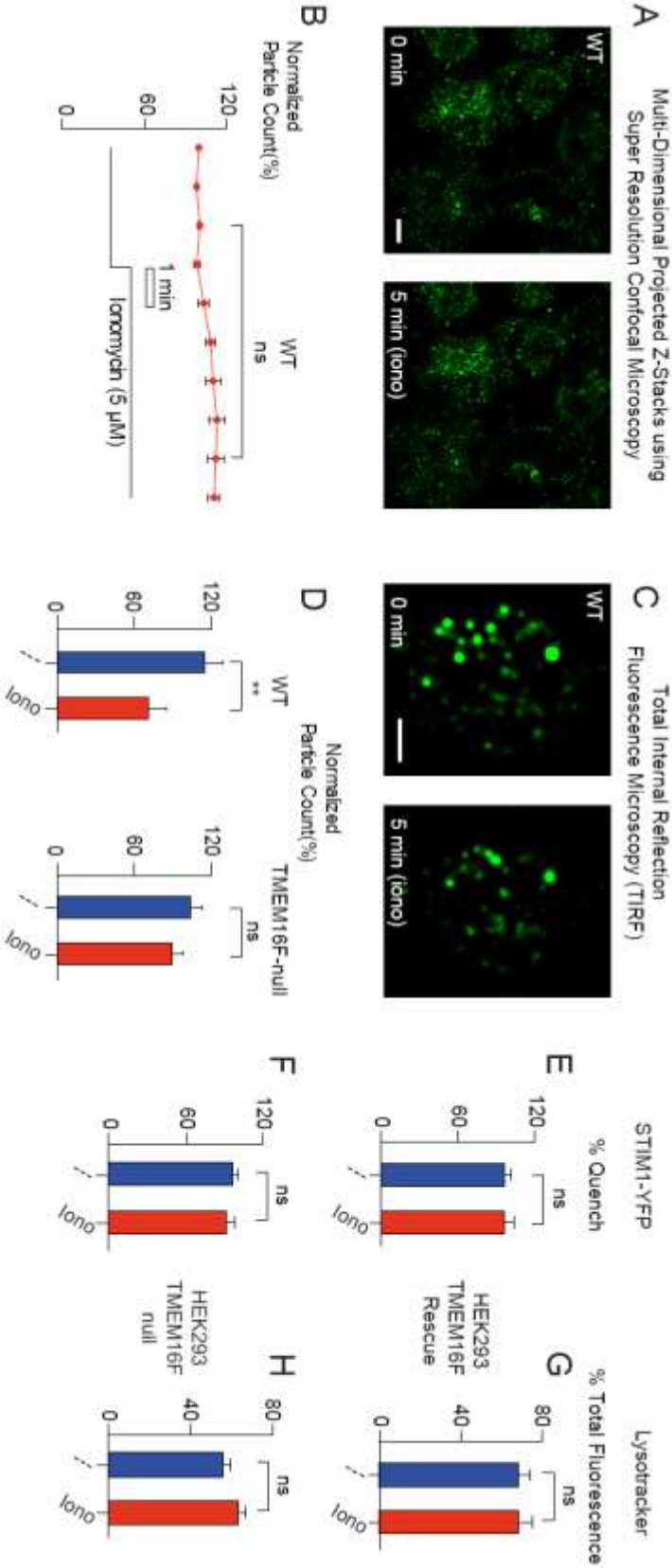

Figure 4

bioRxiv preprint doi: https://doi.org/10.1101/249227; this version posted January 16, 2018. The copyright holder for this preprint (which was not certified by peer review) is the author/funder. All rights reserved. No reuse allowed without permission.

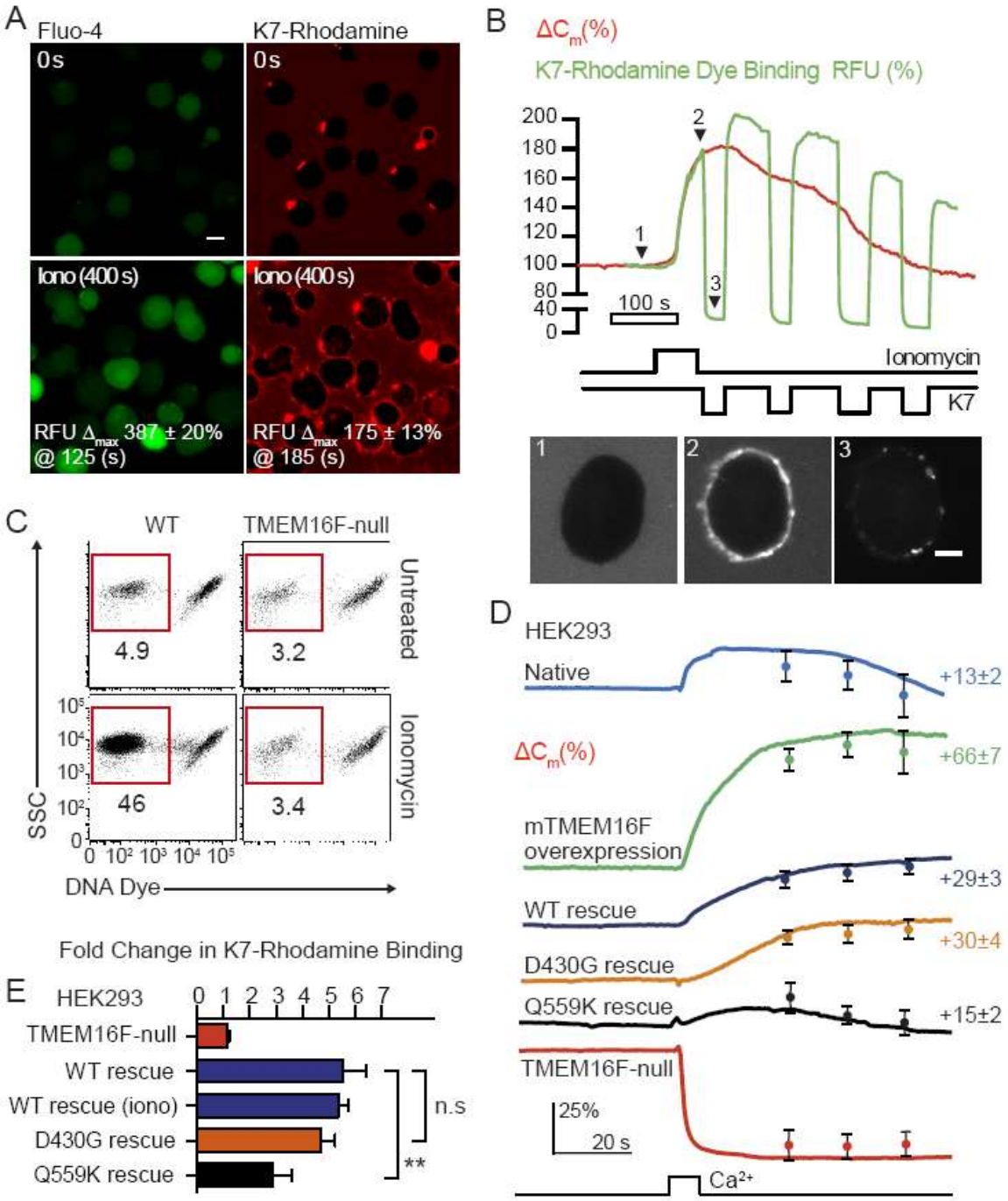

Figure 5

bioRxiv preprint doi: https://doi.org/10.1101/249227; this version posted January 16, 2018. The copyright holder for this preprint (which was not certified by peer review) is the author/funder. All rights reserved. No reuse allowed without permission.

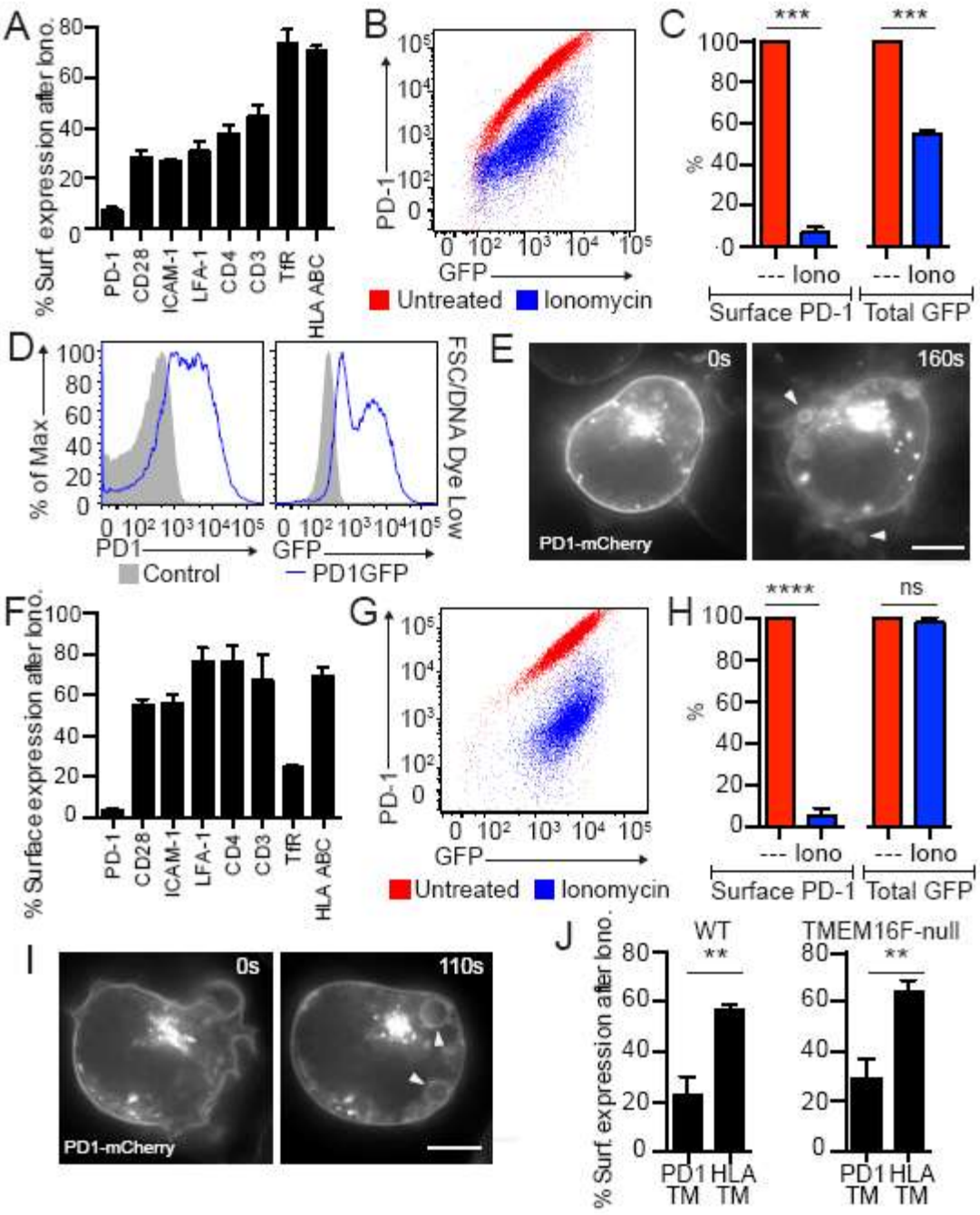

Figure 6

bioRxiv preprint doi: https://doi.org/10.1101/249227; this version posted January 16, 2018. The copyright holder for this preprint (which was not certified by peer review) is the author/funder. All rights reserved. No reuse allowed without permission.

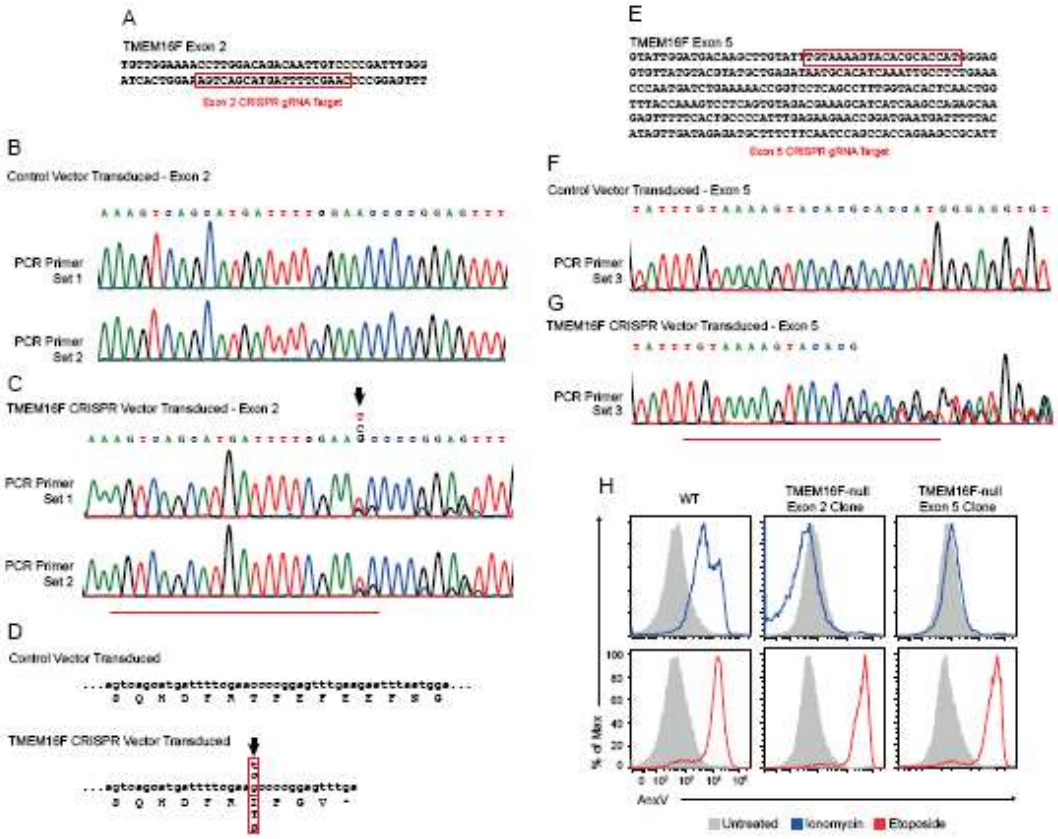

Figure 1. Supplemental File 1

bioRxiv preprint doi: https://doi.org/10.1101/249227; this version posted January 16, 2018. The copyright holder for this preprint (which was not certified by peer review) is the author/funder. All rights reserved. No reuse allowed without permission.

	Wild type	Wild type	Knock-out	Knock-out
	peptides (unique)	% coverage	peptides (unique)	% coverage
TFR1	359 (43)	56	335 (43)	56
Tetraspanin-7	48 (2)	8.8	31 (2)	8.8
CD1c	8 (4)	8.4	7 (4)	11
TMEM16F	13 (6)	10	0	0

Figure 1. Supplemental Table 1.

bioRxiv preprint doi: https://doi.org/10.1101/249227; this version posted January 16, 2018. The copyright holder for this preprint (which was not certified by peer review) is the author/funder. All rights reserved. No reuse allowed without permission.

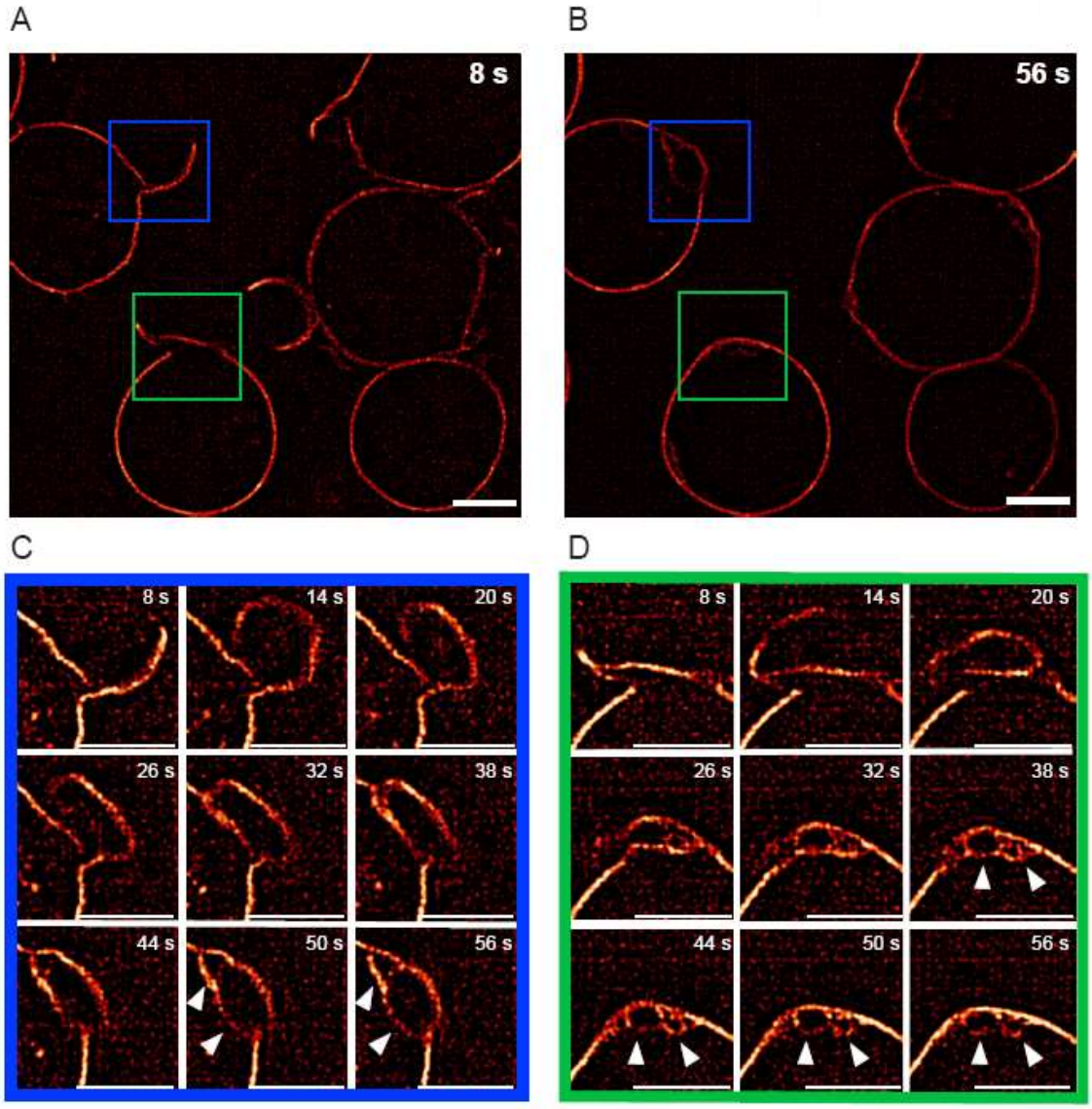

Figure 2. Supplemental File 1.

bioRxiv preprint doi: https://doi.org/10.1101/249227; this version posted January 16, 2018. The copyright holder for this preprint (which was not certified by peer review) is the author/funder. All rights reserved. No reuse allowed without permission.

Figure 5

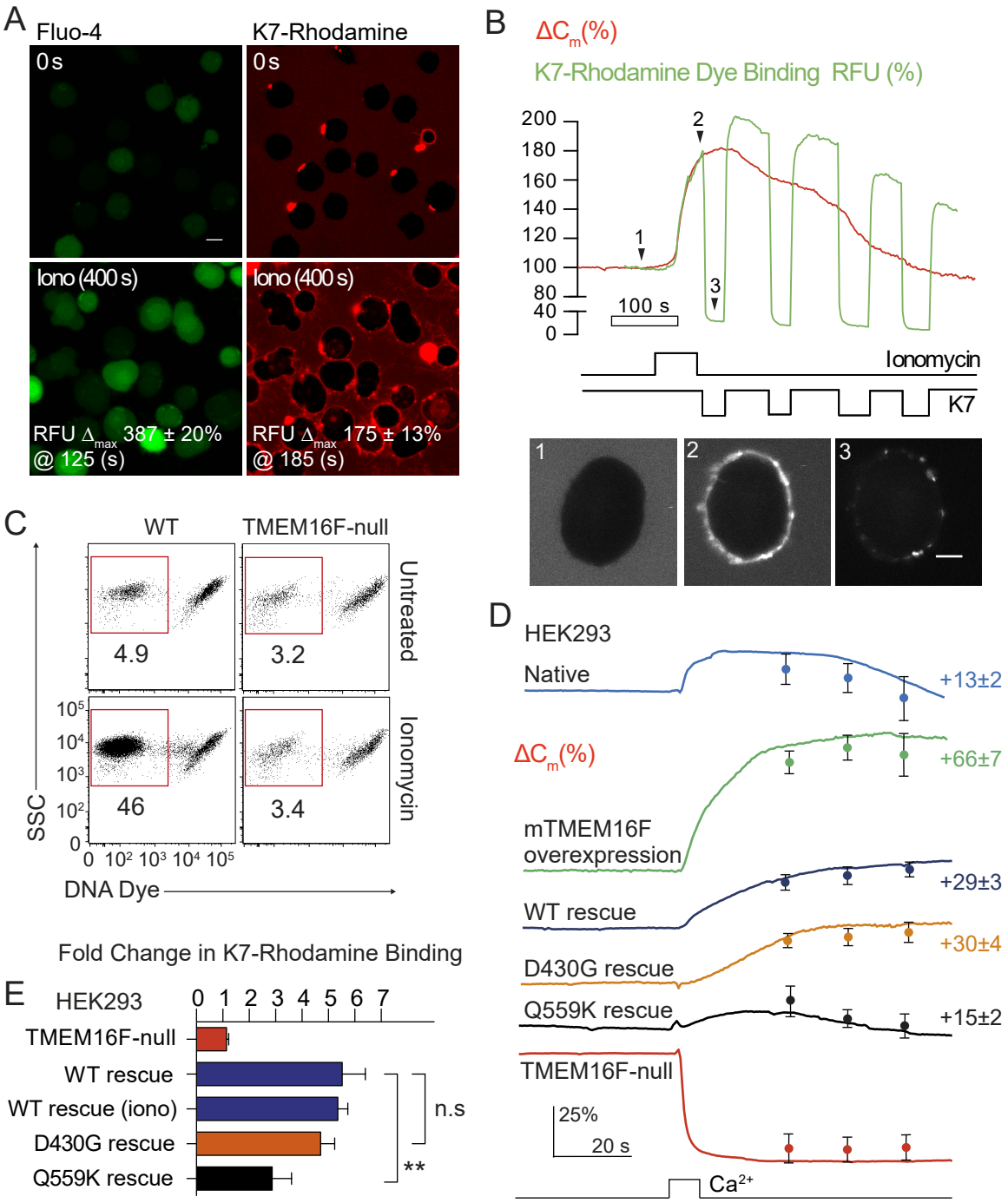

bioRxiv preprint doi: https://doi.org/10.1101/249227; this version posted January 16, 2018. The copyright holder for this preprint (which was not certified by peer review) is the author/funder. All rights reserved. No reuse allowed without permission.

Figure 4

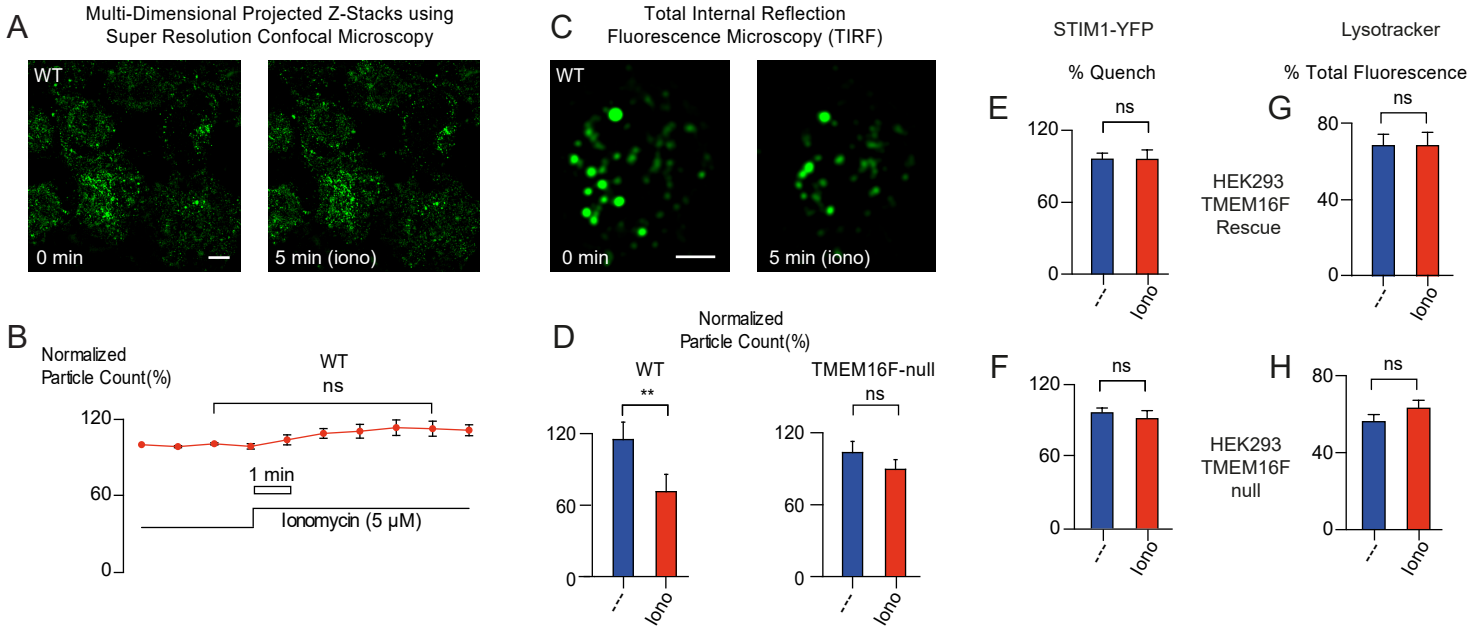

bioRxiv preprint doi: https://doi.org/10.1101/249227; this version posted January 16, 2018. The copyright holder for this preprint (which was not certified by peer review) is the author/funder. All rights reserved. No reuse allowed without permission.

Figure 3

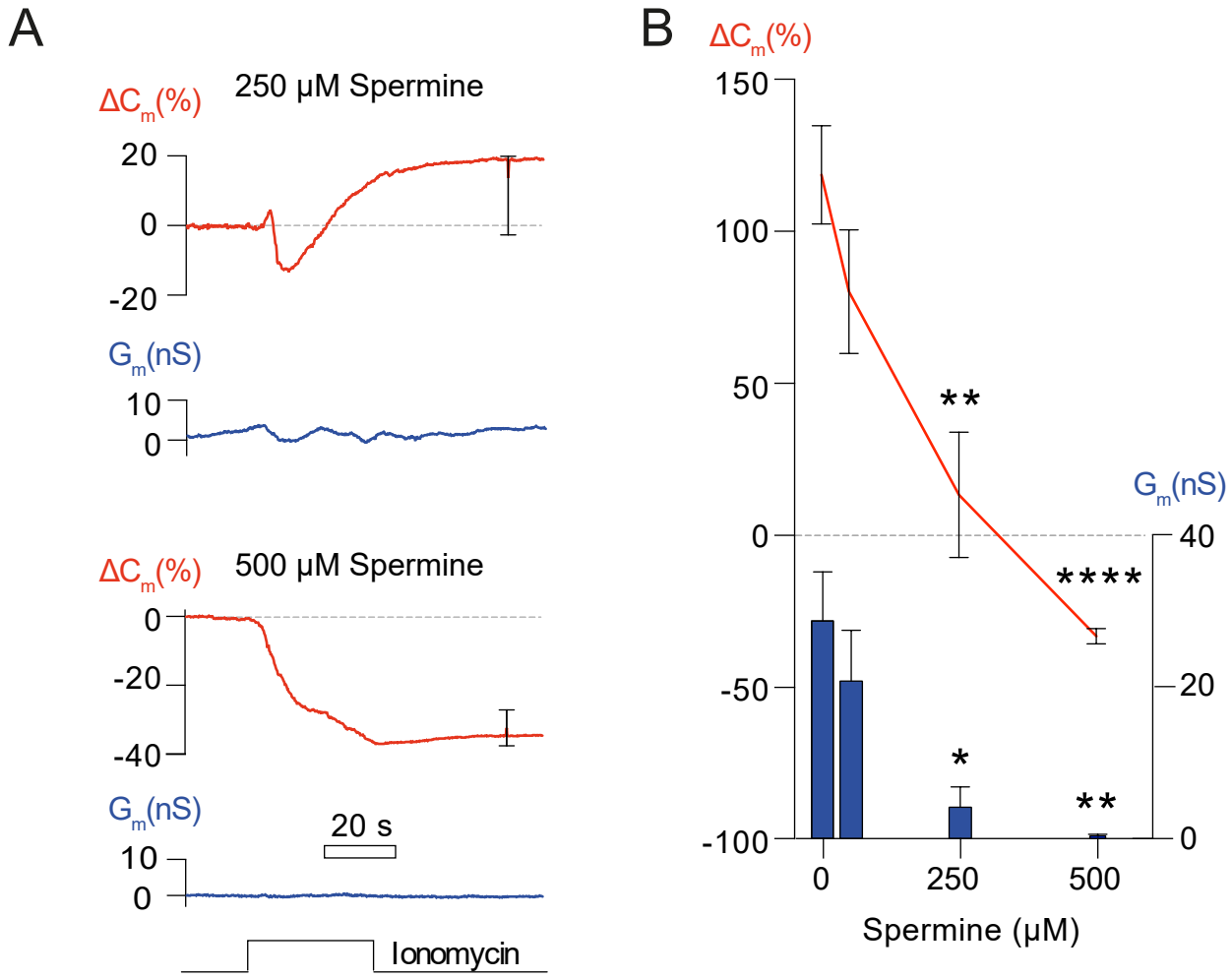

bioRxiv preprint doi: https://doi.org/10.1101/249227; this version posted January 16, 2018. The copyright holder for this preprint (which was not certified by peer review) is the author/funder. All rights reserved. No reuse allowed without permission.

Figure 2

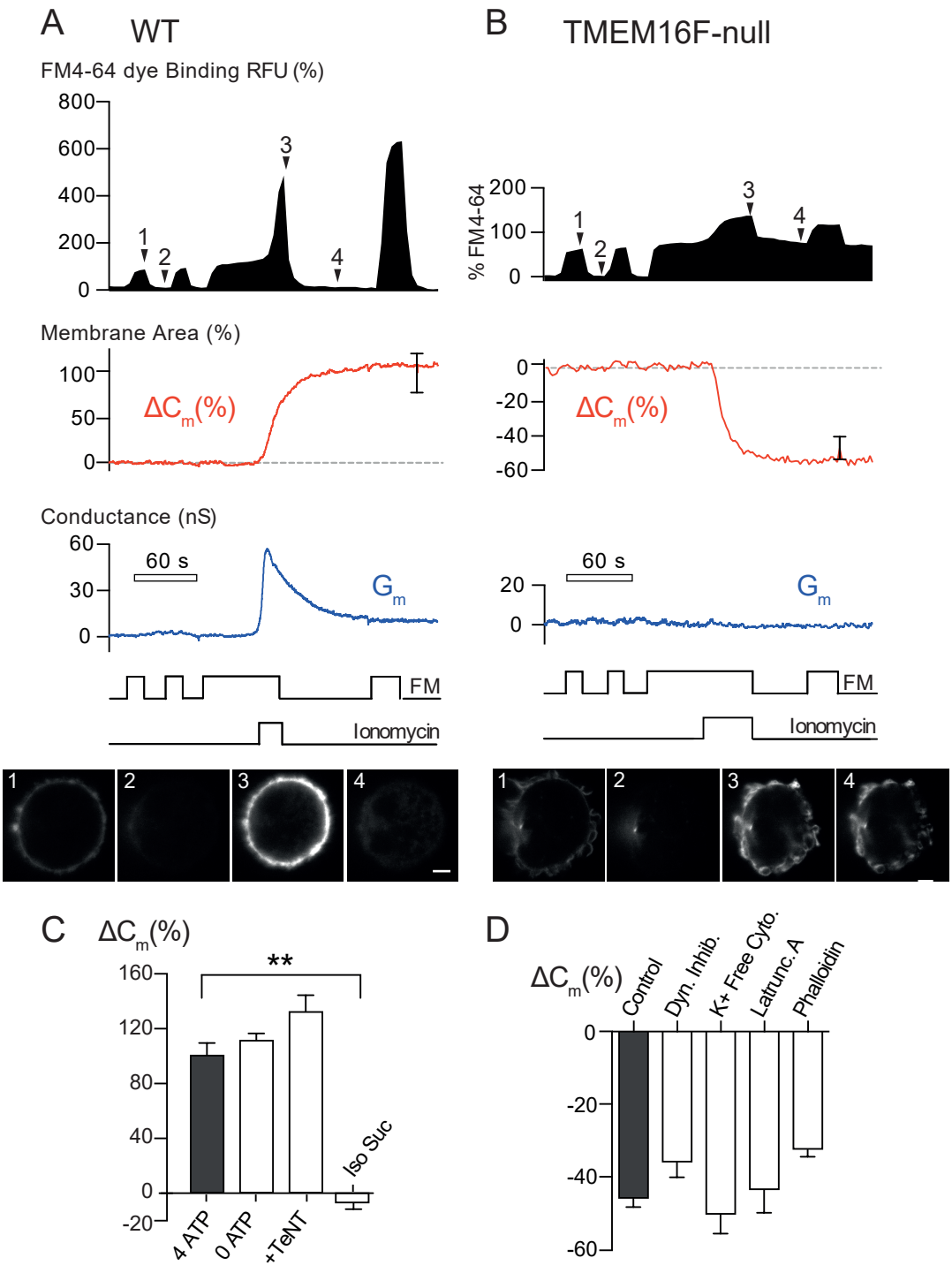

bioRxiv preprint doi: https://doi.org/10.1101/249227; this version posted January 16, 2018. The copyright holder for this preprint (which was not certified by peer review) is the author/funder. All rights reserved. No reuse allowed without permission.

Figure 1

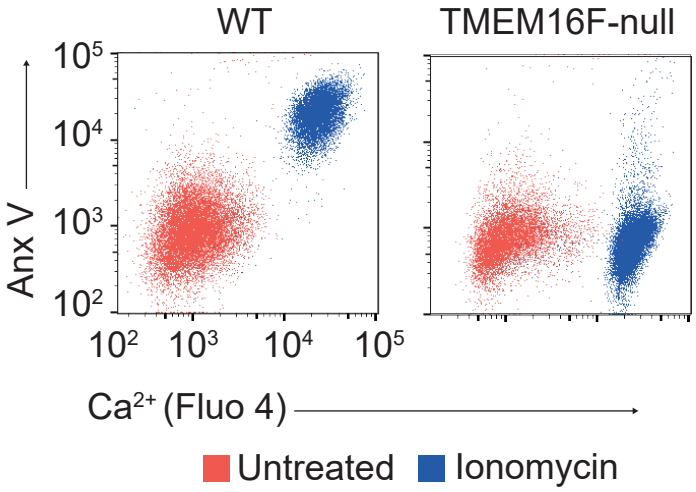

bioRxiv preprint doi: https://doi.org/10.1101/249227; this version posted January 16, 2018. The copyright holder for this preprint (which was not certified by peer review) is the author/funder. All rights reserved. No reuse allowed without permission.
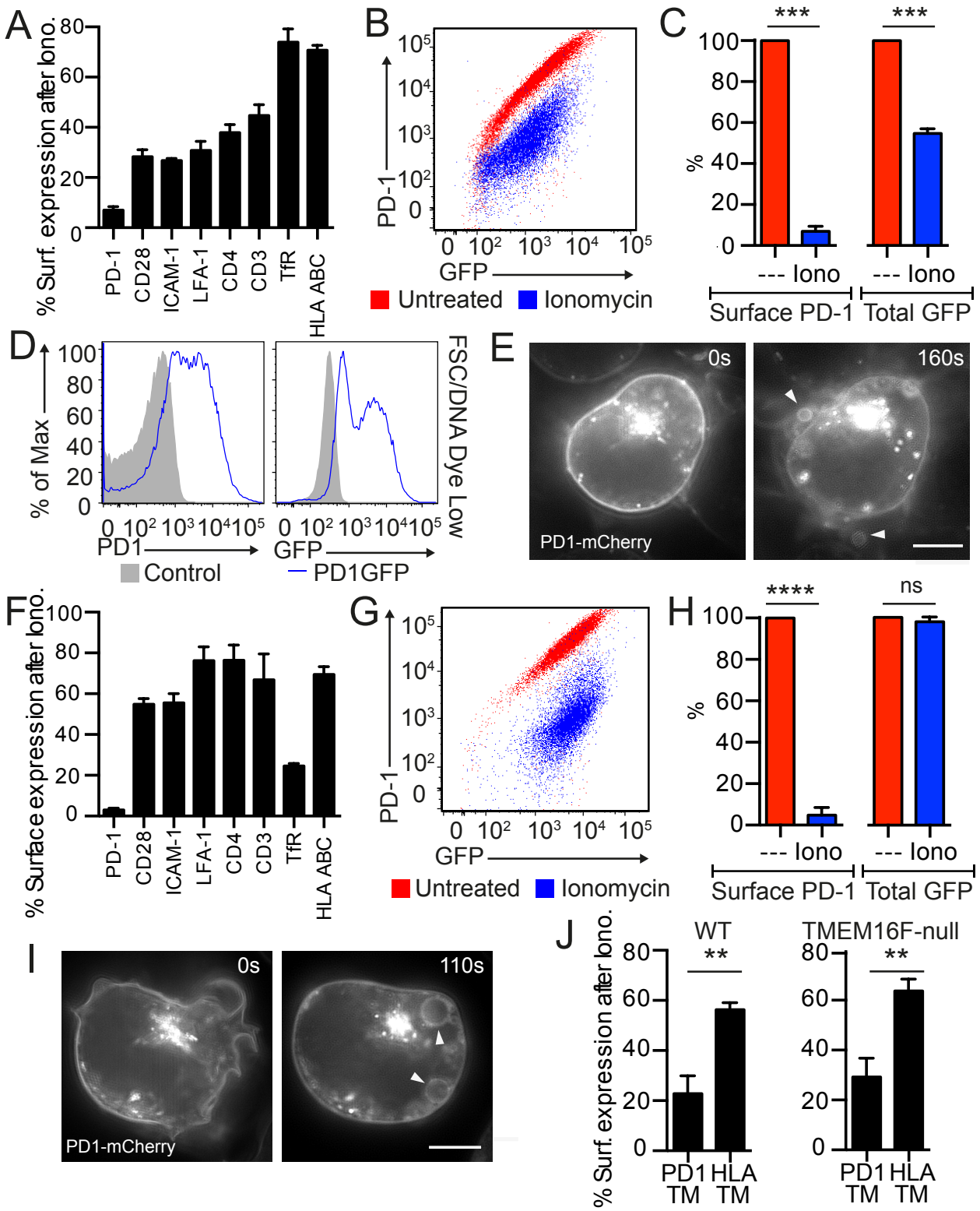
Figure 5